NUMERICAL APPPROXIMATIONS OF THE GREEN'S FUNCTIONS FOR A THEORETICAL MODEL OF AN APERTURE FED STACKED-PATCH MICROSTRIP ANTENNA

THESIS

Ronald E. Erwert
Captain, USAF

AFIT/GE/ENG/90D-19

DEPARTMENT OF THE AIR FORCE
AIR UNIVERSITY
AIR FORCE INSTITUTE OF TECHNOLOGY

Wright-Patterson Air Force Base, Ohio

AFIT/GE/ENG/90D-19

NUMERICAL APPPROXIMATIONS OF THE GREEN'S FUNCTIONS FOR A THEORETICAL MODEL OF AN APERTURE FED STACKED-PATCH MICROSTRIP ANTENNA

THESIS

Ronald E. Erwert
Captain, USAF

AFIT/GE/ENG/90D-19

AFIT/GE/ENG/90D-19

NUMERICAL APPROXIMATIONS OF THE GREEN'S FUNCTIONS FOR A THEORETICAL MODEL OF AN APERTURE FED STACKED-PATCH MICROSTRIP ANTENNA

THESIS

Presented to the Faculty of the School of Engineering

of the Air Force Institute of Technology

Air University

In Partial Fulfillment of the

Requirements for the Degree of

Master of Science in Electrical Engineering

Ronald E. Erwert, B.S.

Captain, USAF

December, 1990

Preface

The purpose of this study was to develop numerical approximations for the Green's functions of a theoretical model of an aperture fed stacked-patch microstrip antenna. Each complex valued Green's functions was approximated by three functional forms. One component of each Green's function was well approximated by a single function. The other component required a piece-wise approximation but with each approximating function valid over the same range, of radial separation, for each function. All the approximations were determined using a least squares curve fitting method and excellent agreement with the original data was obtained. These approximations were given to Capt Leon Irvin for use in a separate effort to determine the patch surface currents using a method of moments analysis. Approximations of this type should provide for a much more computationally efficient method of moments analysis.

I would like to thank my advisor, Major Harry Barksdale, for his help, encouragement, and patience throughout the last year. I would also like to thank the members of my thesis committee, Capt Philip Joseph and Capt Byron Welsh for their help as well as patience and understanding.

The last year and a half have been some of the best and worst times of my life. The association with the members of the LO track will stand as a highlight of my life. In what could have been a competitive race for position in our classes, the members of the LO track were always ready and willing to help and encourage each other. The entire Air Force could benefit from this cooperative type of relationship. On the downside, the last year and a half have been the worst in regards to personal and family life. I would like to give special thanks to my wife Carole, for her love, patience, and understanding over the last year and a half. She sacrificed her career that I might obtain this degree and words will never be able to express my appreciation. I would also like to give thanks to my sons David and Jonathan for doing without "Daddy" much of the time.

In any undertaking, such as a thesis, hind site is always much clearer than foresight. At the outset of this effort an unwritten goal was to rewrite the code used by Nazar to eliminate the

use of commercial software packages. The primary goal was determining the Green's functions approximations. Over the summer a great deal of time was spent investigating different analysis and integration techniques. During this time I seemed to lose sight of the primary goal, obtaining the approximations. When the decision was made to press on, using the routines developed by Nazar, much valuable time had been lost. A clearer plan of attack, with a sequence of important events, might have kept me on track better. The fault rests with the author and not the advisor. Sometimes the lessons hardest learned are the best remembered.

Ronald E. Erwert

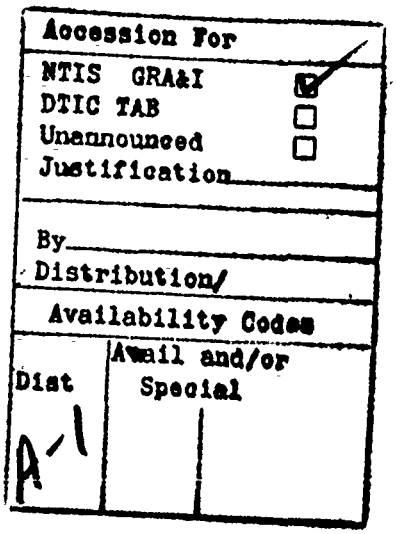

Table of Contents

Page

List of Figures

List of Tables

Abstract

The numerical approximations of the Green's functions for a theoretical model of an aperture fed stacked patch microstrip antenna are presented. The Green's functions approximated are those developed by Nazar (AFIT Thesis GE-89D-37), "Green's Functions for a Theoretical Model of an Aperture Fed Stacked-Patch Microstrip Antenna". Each complex valued Green's function was written as a function of the source-observer separation. The behavior of each Green's function was analyzed, and it was found that they could all be approximated by three separate functions. The approximating functions were either polynomials or rational functions composed of polynomials.

One component could be approximated by a single function over the entire range of radial separations, while the other required a piecewise approximation over the same intervals for each function approximated. The coefficients of the functions were determined by using a least squares curve fitting method and were used in a separate effort (~~AFIT Thesis GE-90D-27~~) to perform a moment method analysis of the antenna. Custom written FORTRAN code was developed to determine the coefficients of the approximations.

Example results for several of the Green's functions approximated are presented. The agreement between the approximations and the original functions was excellent.

NUMERICAL APPROXIMATIONS OF THE GREEN'S FUNCTIONS FOR A THEORETICAL MODEL OF AN APERTURE FED STACKED-PATCH MICROSTRIP ANTENNA

I. Introduction

The microstrip antenna concept was first proposed by Deschamps in 1953 [1]. The concept lay dormant until the early 1970's when there was an immediate demand for low-profile antennas on a new generation of missiles [2] and better theoretical models and manufacturing techniques were developed. Low cost, ease of construction, thin profile, and modular design are among the numerous advantages offered by microstrip antennas. Conformability makes them easy to integrate into the skin of an aircraft or missile without degrading the vehicle aerodynamics. Extensive efforts continue to improve the designs, integrate them into new applications, and develop better analysis techniques to predict antenna performance

1.1 Microstrip Antenna Background

1.1.1 Definition. The basic geometry of a microstrip antenna consists of a conducting strip radiator or patch printed on a grounded dielectric substrate (see Figure 1). The antenna input or feed can be either a coaxial cable or a microstrip. The antenna patch conductors can in principle be any shape but are usually rectangular or circular to simplify analysis and performance prediction. Generally the substrate dielectric constant should be low ($\varepsilon \approx 2.5$) to enhance the fringe fields which account for the radiation [1].

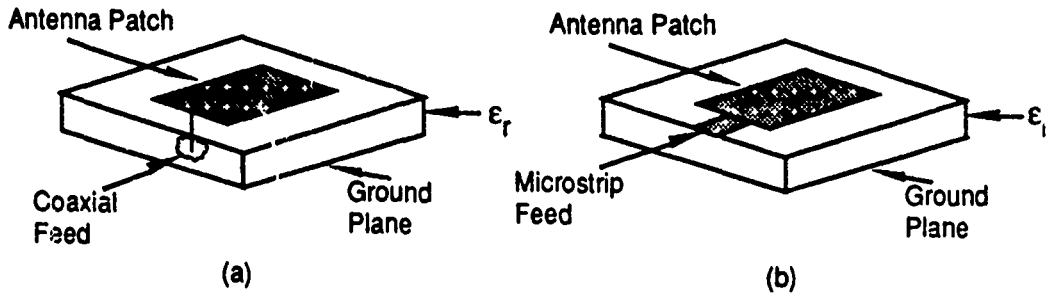

Figure 1. Microstrip Antennas with (a) Coaxial Feed and (b) Microstrip Feed [3].

1.1.2 Advantages. Compared to conventional antennas, microstrip antennas have numerous advantages and can be used in a wide variety of applications over a frequency range of approximately 100 MHz to 50 GHz. Some of the major advantages are [1]:

- light weight, low volume, low profile planar configurations which can be made conformal
- low fabrication cost, readily amenable to mass production
- can be made thin; hence they do not perturb the aerodynamics of the host aerospace vehicles
- the antennas may be easily mounted on missiles, rockets and satellites without major alterations
- microstrip antennas are compatible with modular designs (Solid state devices such as oscillators, amplifiers, variable attenuators, switches, modulators, mixers, phase shifters, etc. can be added directly to the antenna substrate board)
- feed lines and matching networks may be fabricated simultaneously with the antenna

1.1.3 Disadvantages. Unfortunately microstrip antennas do have some disadvantages compared to conventional antennas such as [1]:

- narrow bandwidth
- loss, hence somewhat lower gain
- most microstrip antennas radiate into a half plane
- poor end-fire radiation performance
- poor isolation between the feed and radiating elements

1.2 Problem Background

As previously stated, narrow bandwidth is one of the disadvantages of microstrip antennas. The bandwidth of the antennas shown in Figure 1 is typically 1-5% of the resonant frequency. Increasing the substrate thickness can increase the bandwidth but any bandwidth gains are offset by loss, radiation, and impedance mismatch problems [3].

Captain James Nazar developed an analytical model of a configuration combining two bandwidth improving techniques, aperture feeding from a microstrip line and using stacked patch radiating antenna elements. A picture of this aperture fed stacked-patch microstrip antenna is shown in Figure 2. In his thesis he presented a theoretical model for this antenna using the mixed potential integral equation (MPIE) approach. The Green's functions associated with the vector and scalar potentials are evaluated in the spatial domain using stratified media theory. He outlines a method of moments technique to solve for the currents but no actual solutions for the currents are calculated.

The Green's functions developed are expressed in the form of Sommerfeld integrals. The moment method analysis requires surface integration of the Green's functions over the source and observer coordinates. The Green's function integrands are dependent on the radial separation between the source and observer. To numerically evaluate the integrals of each Green's function at every value of radial separation required in the surface integrations would be extremely time consuming. Nazar proposed numerically evaluating the integral Green's functions over a finite number of radial separations and interpolating to find the intermediate values. He states polynomial averaging may be an acceptable interpolation technique [3].

1.3 Problem Statement

In this thesis, a subset of the Green's functions developed by Nazar will be numerically evaluated at a finite number of observer-source radial separations and approximations for each

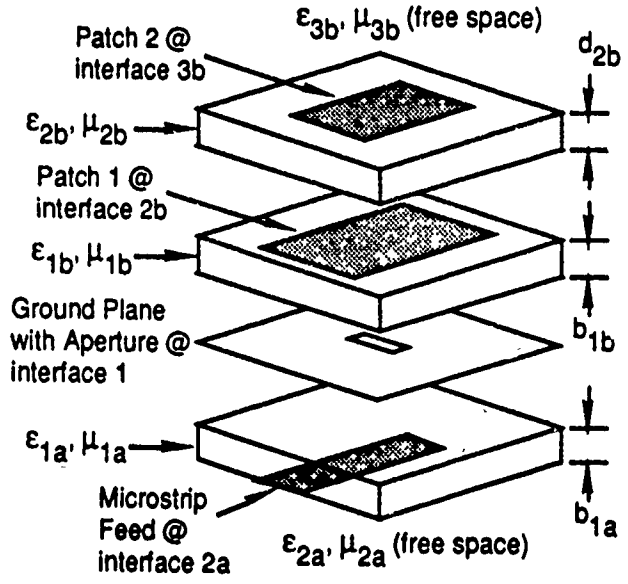

Figure 2. Aperture Fed Stacked-Patch Microstrip Antenna [3].

Green's function will be developed which can then be used in a tractable method of moments analysis.

1.4 Research Objectives

The main goal of this research is to further develop a mathematical model suitable to analyze an aperture fed stacked-patch microstrip antenna as displayed in Figure 2. The Green's functions, previously developed, are in the form of Sommerfeld integrals which will be solved numerically and approximated by simpler functions. These Green's function approximations will be used in a concurrent thesis effort, by Captain Irvin [4], to perform a method of moments analysis to determine the various currents of the antenna. Captain Terry [5] is building and measuring the radiation characteristics of an aperture fed stacked-patch microstrip antenna. The culmination of these thesis efforts should be a working and verified analytical model of the antenna.

1.5 *Research Questions*

Answers to the following questions will be found:

1. What are the form functions necessary to accurately model the Green's functions?
2. How well do these functions approximate the original Green's function?

1.6 *Assumptions*

Because this thesis effort is a continuation of Nazar's work, the same simplifying assumptions were made about the material parameters to make the mathematical analysis tractable. Each dielectric is considered isotropic, homogeneous, and lossless. The dielectric layers and ground plane are considered infinite sheets. The ground plane and antenna patch conductors are infinitely thin, perfect electrical conductors, while the dielectric layers have finite thickness. Finally, the Green's functions derived by Nazar were assumed correct.

1.7 *Scope and Limitations*

Only the aperture fed stacked-patch microstrip antenna was analyzed. The unique Green's functions derived by Nazar were evaluated numerically and approximated by appropriate polynomials. Once these functions were determined, the coefficients were given to Capt Irvin for use in a method of moments analysis to determine the electric and magnetic currents of the antenna.

1.8 *Thesis Organization*

The rest of this document is organized in the following manner. Chapter II is a review of several current articles on aperture fed microstrip antennas, stacked-patch microstrip antennas, aperture fed stacked-patch microstrip antennas, and the method of full wave analysis. Chapter III contains the theory necessary to develop the Green's functions in the theoretical model used to analyze this antenna. Chapter IV presents an explanation of what functions are approximated,

what the approximations are and how well the functions approximate the Green's functions. The conclusions and recommendations are discussed in Chapter V. Finally the components of the vector potential derived in Chapter III as well a complete list of the Green's functions used in the model are contained in appendices.

II. Literature Review

This literature review summarizes current work on microstrip antennas. Since this thesis effort concentrates on further development of a theoretical model for an aperture fed stacked-patch microstrip antenna, only current reports on aperture fed microstrip antennas, stacked patch microstrip antennas, aperture fed stacked-patch microstrip antennas, and full wave analysis techniques will be summarized. The final work reviewed is Captain James Nazar's thesis, the departure point for this thesis effort.

2.1 Aperture Coupled Antennas

In 1985 D. M. Pozar [6] presented a new technique for feeding microstrip antennas. He proposed coupling a microstrip patch on a substrate to a microstrip line feed located on a parallel substrate via an aperture in the ground plane separating the two substrates (see Figure 3). To make the feedline location easier to visualize, the feed substrate in Figure 3 is shown transparent. Pozar cited three advantages of an aperture coupled configuration:

1. The configuration is well suited for monolithic phased arrays, where active devices can be integrated on, for example, a gallium arsenide substrate with the feed network, and the radiating elements can be located on an adjacent (low-dielectric constant) substrate, and coupled to the feed network through apertures in the ground plane separating the two substrates. The use of two substrates thus avoids the deleterious effect of a high-dielectric-constant substrate on the bandwidth and scan performance of a printed antenna array.
2. No radiation from the feed network can interfere with the main radiation pattern, since a ground plane separates the two mechanisms.
3. No direct connection is made to the antenna elements, so problems such as large probe self reactances or wide microstrip line (relative to patch size), which are critical at millimeter-wave frequencies, are avoided.[6]

Pozar designed a prototype antenna using small hole coupling theory and a cavity model for the patch. No specific bandwidth performance results were cited, but he did report that the patterns in the principle radiation planes were basically the same as for a microstrip antenna with same geometry. Also radiation from the feed side of the antenna was negligible.

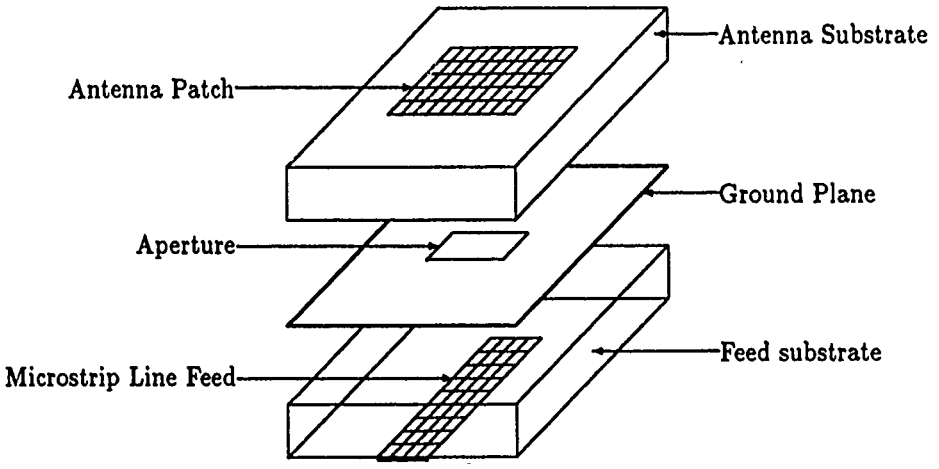

Figure 3. Aperture Coupled Microstrip Antenna.

Sullivan and Schaubert [7] took Pozar's concept and developed an exact mathematical model for an aperture fed microstrip antenna with one radiating antenna patch. They formulated coupled integral equations by using the Green's functions for grounded dielectric slabs. Their analysis included all the coupling, radiation and surface wave effects for both substrates. In their analysis they invoked the equivalence principle, closed off the aperture and replaced it with magnetic surface currents $\mathbf{M_s}$ located just above and below the ground plane (see Figure 4). To ensure continuity of the tangential electric field across the aperture, the magnetic currents are of equal magnitude but oppositely directed. The space below the ground plane ($z < 0$) is designated as region a and the region above ($z > 0$) as region b. The known incident current distribution on the feedline is $\mathbf{J_{inc}}$, the scattered current distribution on the feedline is $\mathbf{J_f}$ and the current distribution on the patch is $\mathbf{J_p}$. The electric and magnetic fields in each region can then be written as the summation of the contributions from each source:

$$\mathbf{E_a^{tot}} = \mathbf{E_a}(\mathbf{J_{inc}}) + \mathbf{E_a}(\mathbf{J_f}) + \mathbf{E_a}(\mathbf{M_s})$$

$$\mathbf{H_a^{tot}} = \mathbf{H_a}(\mathbf{J_{inc}}) + \mathbf{H_a}(\mathbf{J_f}) + \mathbf{H_a}(\mathbf{M_s})$$

$$\mathbf{E_b^{tot}} = \mathbf{E_b}(\mathbf{J_p}) - \mathbf{E_b}(\mathbf{M_s})$$

$$\mathbf{H_b^{tot}} = \mathbf{H_b}(\mathbf{J_p}) - \mathbf{H_b}(\mathbf{M_s})$$

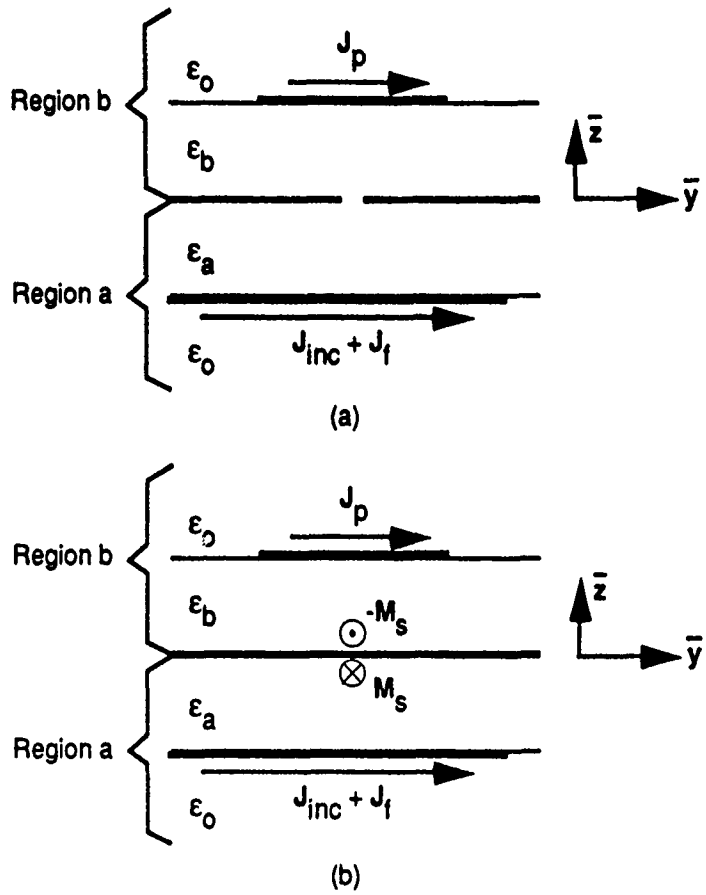

Figure 4. Antenna and Feed with Incident and Induced Currents. (a) Original problem. (b) Equivalent problem. [3, 7].

By enforcing the boundary conditions they obtained three coupled integral equations for the unknown currents $\mathbf{J_f}, \mathbf{M_s}$ and $\mathbf{J_p}$. The equations were then solved using a Galerkin moment method procedure. The analysis was simplified by assuming the electric currents on the antenna patch and stripline were only in the y-direction and the aperture was electrically shorted and replaced by magnetic currents confined to the x-direction. The expression obtained for $\mathbf{M_s}$ was not quite exact because one material parameter must be determined from empirical data. The authors verified their results by comparing calculated to measured input impedance for several different combinations of dielectric constant, dielectric thickness and aperture position and obtained good agreement between predicted and measured performance.

Tsao *et al.* [8] reported the results from the design and testing of several aperture fed stacked-patch microstrip antennas. A test model with a single input feed network achieved a 19.2 percent bandwidth at 3.9 GHz with an input voltage standing wave ratio less than two. A two-input-port model designed for dual polarization achieved a 23 percent bandwidth at 3.74 GHz with an input VSWR less than two. No exact analysis was presented but the authors did demonstrate that an aperture fed stacked-patch microstrip antenna can yield higher bandwidth than a single patch microstrip antenna.

Das [9] studied the general configuration of printed antennas fed by planar transmission lines in a multilayered substrate geometry by analysis using a full wave spectral domain moment method. In his model he developed a complete set of full wave spectral domain Green's functions for a multilayered geometry. One particular configuration he studied was an aperture fed stacked-patch antenna. He verified his analysis by using a waveguide simulator and reported a bandwidth of 11 to almost 17 percent depending upon the primary patch size.

In a recent article Pozar [10] modeled an infinite phased array of aperture coupled microstrip patches. His solution used the exact Green's functions for the dielectric substrates in a spectral domain moment method approach. The coupling of one aperture in the infinite array to its as-

sociated feedline is found, and an equivalent series impedance is determined. The model assumes no coupling between the feed lines themselves as long as they do not come within a few substrate thicknesses of each other. A waveguide simulator was used to verify the theory. The agreement between measured and calculated impedance results was good.

2.2 Analysis of Microstrip Antennas

The electromagnetic fields radiated by a microstrip antenna are found by solving the integral equations for the currents on the feed elements and the antenna patch(s). Mosig [11] describes a mixed potential integral equation (MPIE) technique applied to microstrip structures which can be used to solve for the currents. In this method he uses Green's functions associated with the scaler and vector potentials which are calculated by using stratified media theory and are expressed as Sommerfeld integrals. The author solves the MPIE in the space domain to keep a good physical insight to the problem. The MPIE is numerically stable and can be solved with efficient algorithms. The formulation of these equations provides a powerful and flexible technique because contributions from coupling, dispersion, radiation losses and surface waves are included. The technique can be extended to multilayered substrates and multiple conductors at different levels (stacked patches) by making suitable modifications to the Green's functions and increasing the number of unknowns.

Additional insight into using the MPIE is provided by an earlier paper by Mosig and Gardiol [12]. The authors develop in detail the spatial Green's functions associated with microstrip structures. These Green's functions correspond to the fields and potentials created by a horizontal electric dipole placed on the air/dielectric interface and are expressed as Sommerfeld integrals. The situation where both the source and observer are located on the same plane is studied extensively. Numerical methods to evaluate the Sommerfeld integrals in this situation are reviewed, and several techniques introduced and discussed in detail.

Analytical techniques applicable to stratified media were needed to develop the model for the

antenna studied in this thesis. Mosig indicated the MPIE can be used for stratified media but he derived the Green's functions using only the horizontal electric dipole (HED) and a point charge and did not derive the Green's functions for stratified media [11]. Kong developed the integral expressions for the electric and magnetic fields for both the HED and the horizontal magnetic dipole (HMD) in both infinite and semi-infinite stratified media [13]. As discussed later, Nazar extracted the HED and HMD Green's functions for stratified media from Kong's integral field expressions [3]. The Green's functions for the HMD were needed to determine the fields radiated by the magnetic currents used to close off the aperture in the ground plane.

Das and Pozar derived a generalized, two dimensional, spectral-domain Green's function completely defining the field inside a multilayered dielectric structure due to a current element located between any two layers. They derive their solution by solving a "standard" form containing the current element located on the interface between any two layers and using an iterative algorithm to take care of additional layers. Another iterative algorithm is then used to find the field in any layer in terms of the field expressions in the two layers of the "standard" form. The locations of the poles of the Green's function are predicted, and an asymptotic form is derived along with the asymptotic limit. From their analysis they draw the following conclusions:

1. The convergence of the numerical solution of the Green's functions is much faster when the source and observer are on different planes than when they are coplanar.
2. The numerical convergence to the asymptotic limit is much faster for thicker dielectric layers.
3. The convergence of the numerical solution is much faster for structures with a ground layer than for structures without a ground plane [14].

Most of the exact analysis of microstrip antennas has concentrated on deriving the Green's functions using only horizontal dipole sources such as the HED and HMD. Hall and Mosig [10] applied the MPIE approach to vertical monopoles embedded in a dielectric substrate media. The vector and scalar potentials were written in terms Sommerfeld integrals and evaluated using techniques similar to those developed for horizontal dipoles in microstrip antennas. The analysis was

verified by comparing measured and calculate impedance data for a monopole embedded in Teflon. Good results were obtained indicating this method may be useful for modeling the coaxial feed for a microstrip patch antenna.

Barlatey *et al.* analyzed a stacked patch microstrip antenna using the MPIE approach. They provided a complete and rigorous treatment of the Green's functions for the potentials in the space domain, created by a HED located at any of the dielectric interfaces of a multilayered structure. The surface waves which can arise in such a structure were characterized numerically. An approximate formula for the value of the propagation constant of the dominant TM_0 mode was given, and conditions necessary to ensure the absence of higher order modes were specified. The MPIE was solved with a Galerkin method of moments procedure. They show that the introduction of auxiliary variables greatly reduces computation time. Theoretical results for the input impedance of a two-layer patch agreed well with measurements. The authors estimate one configuration would have a bandwidth greater than 15 percent for a VSWR of two or less.

2.3 Nazar's Thesis[3]

Nazar developed a theoretical model for the analysis of an aperture fed stacked-patch microstrip antenna. The mixed potential integral equation (MPIE) approach was used. The aperture was closed by using opposing magnetic currents on each side of the ground plane. As noted before, Nazar derived the stratified media Green's functions using both the HED and HMD. The necessary Green's functions associated with the vector and scalar potentials were evaluated in the spacial domain to keep a good physical insight to the problem. The Green's functions are expressed as Sommerfeld integrals. A method of moments technique to solve for the currents of the antenna is outlined but no actual solutions are calculated. The Sommerfeld integral in the Green's functions were analyzed and found to have the following characteristics: complex,oscillatory integrands; singularities; surface waves; and semi-infinite integration intervals. He also developed several inte-

gration techniques to deal with these characteristics. Example calculations for several of the Green's functions were performed. The cut-off frequencies for the surface waves were determined and he found that for the proper choice of material parameters only one surface wave mode propagates. Example Green's functions were evaluated with sample results reported.

2.4 Summary

Microstrip antenna research continually produces innovative designs and more elaborate analysis techniques. Work by Pozar, Sullivan and Schaubert, Tsao *et al.*, Das, and Barlatey *et al.* have shown the feasibility of using aperture coupling and stacked patches to increase the bandwidth of microstrip antennas. Sullivan and Schaubert, Mosig and Gardiol, Kong, and Das and Pozar developed analytical techniques to rigorously calculate the solutions for microstrip antennas in stratified media. Hall and Mosig applied the MPIE approach to vertical monopoles embedded in a dielectric substrate. Nazar developed the Green's functions for an aperture fed stacked-patch microstrip antenna. Solving these Green's functions numerically in an efficient manner will allow their use in a method of moments analysis to determine the antenna currents. The complete analytical model for this antenna can then be used to define frequency, bandwidth, and radiation characteristics and thus develop criteria for the efficient design of this antenna.

III. Theory

3.1 Analysis Overview

The goal of this analysis is to find the induced electric currents on the two antenna patches given an assumed magnetic surface current over the aperture. These currents can be used to determine the antenna operating characteristics such as resonant frequency, input impedance, bandwidth, and radiation pattern. The various antenna currents are illustrated in Figure 5. The electric currents are labeled as $\mathbf{J_{inc}}$ for the feedline current; $\mathbf{J_f}$ is the feedline scattered current; $\mathbf{J_2}$ is the primary patch current; and $\mathbf{J_3}$ is the parasitic patch current. The equivalence principle [15] can be used to close off the aperture and replace it with opposing magnetic surface currents $\mathbf{M_1}$ located just above and below the ground plane. The opposing magnetic currents ensure continuity of the tangential electric field through the aperture [7]. Though only x-directed electric and y-directed magnetic currents are shown in Figure 5, the analysis includes all currents in the xy-plane. The total electric and magnetic fields in regions *a* and *b* can be written as the summation of the contributions from each source:

$$\mathbf{E_a^{tot}} = \mathbf{E_a}(\mathbf{J_{inc}}) + \mathbf{E_a}(\mathbf{J_f}) + \mathbf{E_a}(\mathbf{M_1}) \quad (1)$$

$$\mathbf{H_a^{tot}} = \mathbf{H_a}(\mathbf{J_{inc}}) + \mathbf{H_a}(\mathbf{J_f}) + \mathbf{H_a}(\mathbf{M_1}) \quad (2)$$

$$\mathbf{E_b^{tot}} = \mathbf{E_b}(\mathbf{J_2}) + \mathbf{E_b}(\mathbf{J_3}) - \mathbf{E_b}(\mathbf{M_1}) \quad (3)$$

$$\mathbf{H_b^{tot}} = \mathbf{H_b}(\mathbf{J_2}) + \mathbf{H_b}(\mathbf{J_3}) - \mathbf{H_b}(\mathbf{M_s}) \quad (4)$$

In this analysis a somewhat simplified model is used. Rather than using $\mathbf{J_{inc}}$ as the known input, the magnetic surface current across the aperture is assumed known. Thus only the two patch currents $\mathbf{J_2}$ and $\mathbf{J_3}$ need be solved for. To determine these currents, only expressions for the electric field need to be derived.

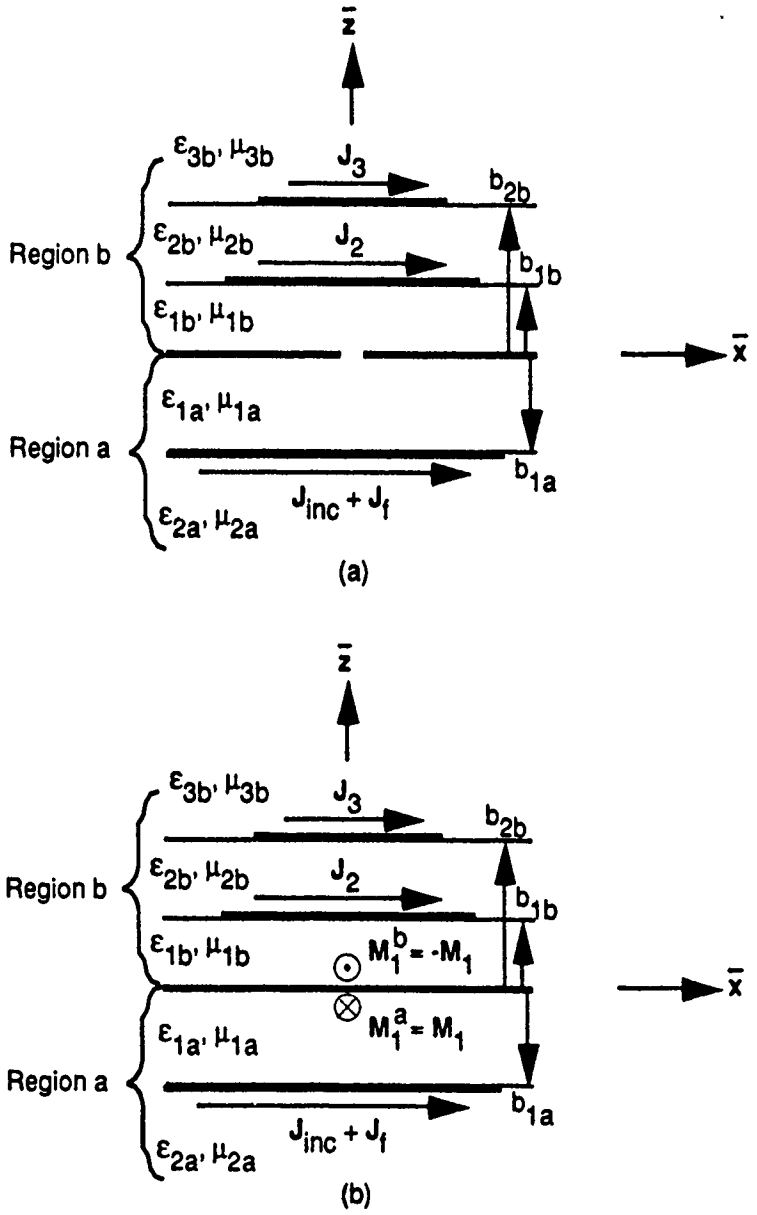

Figure 5. Stacked Patch Antenna and Feed with Incident and Induced Currents [3]. (a) Original Problem. (b) Equivalent Problem.

The electric fields in the problem can be expressed using the mixed potential integral equation (MPIE) and solved in the space domain. Harrington discussed using both vector and scalar potentials (mixed potentials) to solve scattering and antenna problems [16]. Mosig applied the MPIE to microstrip antennas [11] and Nazar applied them to the aperture fed stacked patch structure [3].

The electric fields due to the electric and magnetic sources, respectively, are derived from the scalar and vector potentials

$$\mathbf{E} = -j\omega\mathbf{A} - \nabla V \tag{5}$$

$$\mathbf{E} = -\frac{1}{\epsilon}\nabla \times \mathbf{F} \tag{6}$$

where $\mathbf{A}$ is the magnetic vector potential, V is the electric scalar potential, $\mathbf{F}$ is the electric vector potential, and $j=\sqrt{-1}$.

Equation (5) assumes only electric sources are present and Eq (6) assumes only magnetic sources. The vector and scaler potentials can be expressed using the corresponding Green's function as superposition integrals of the current and charge densities.

$$\mathbf{A}(\rho) = \int_{s'} \overline{\overline{G}}_A(\rho|\rho') \cdot \mathbf{J}(\rho')ds' \tag{7}$$

$$V_q(\rho) = \int_{s'} G_q(\rho|\rho')q(\rho')ds' \tag{8}$$

$$\mathbf{F}(\rho) = \int_{s'} \overline{\overline{G}}_F(\rho|\rho') \cdot \mathbf{M}(\rho')ds' \tag{9}$$

with the dot in Eqs (7) and (9) indicating a dot product of the dyadic Green's function with the vector surface current. The radial positions of the observer and source respectively, from the z-axis are represented by ρ and ρ'. The continuity equation relates the electric current and charge density.

$$\nabla \cdot \mathbf{J} + j\omega q = 0 \tag{10}$$

The electric field in region b (the half space into which the antenna radiates) is described by substituting Eq (7) through (10) into Eqs (5) and (6). Two coupled integral equations are then obtained for the two unknown currents $\mathbf{J_2}$ and $\mathbf{J_3}$ by enforcing the boundary conditions of Table 1. The remaining boundary conditions such as conditions on the normal and tangential fields at the dielectric interfaces, are incorporated in the construction of the Green's functions.

Table 1. MPIE Boundary Conditions [3]

1) $\mathbf{E}^{tan} = 0$ on antenna patch 1
2) $\mathbf{E}^{tan} = 0$ on antenna patch 2

In developing a mathematical model the first step is to determine the expressions for the vector and scalar potentials from which the Green's functions are constructed. The MPIEs satisfying the boundary conditions in Table 1 are then formulated and can be solved for the current and charge distribution by a moment method solution. Throughout the analysis a time dependance of $e^{j\omega t}$ is assumed.

3.2 Vector and Scalar Potentials

By definition the Green's functions are potentials created by a unit source which is an electric or Hertz dipole located on of the patches or an equivalent magnetic source located across the aperture in the ground plane. The superposition principle applies in a linear system and the potentials of any finite source can be determined by representing the source as a continuum of elementary dipoles and integrating the contributions of all the elementary sources [17]. The method of Green's functions for arbitrary microstrip sources was developed by Mosig and Gardiol [12, 17]. However, they only constructed Green's functions for a single dielectric layer antenna, with only electric sources on the dielectric-air interface and the dielectric permeability fixed at the free space value. Nazar [3] extended these results to model an aperture fed stacked-patch structure with

two dielectric layers with different permittivities *and* permeabilities; with electric sources at the dielectric-dielectric and dielectric-air interfaces; and with equivalent magnetic sources at the ground plane-dielectric interfaces.

3.2.1 HED at Interface 2b [3]. The first step in analyzing this structure is to determine the magnetic vector potential created by a HED having a unit moment ($Idx = 1$ A m) along the x-axis at the interface of dielectrics 1b and 2b (see Figure 6) [3]. The resulting Green's functions can be used in Eqs (7) and (8) along with Eq (5) to obtain the **E** fields of the structure for an arbitrary distribution of sources on interface 2b. The x and z components of the magnetic vector potential

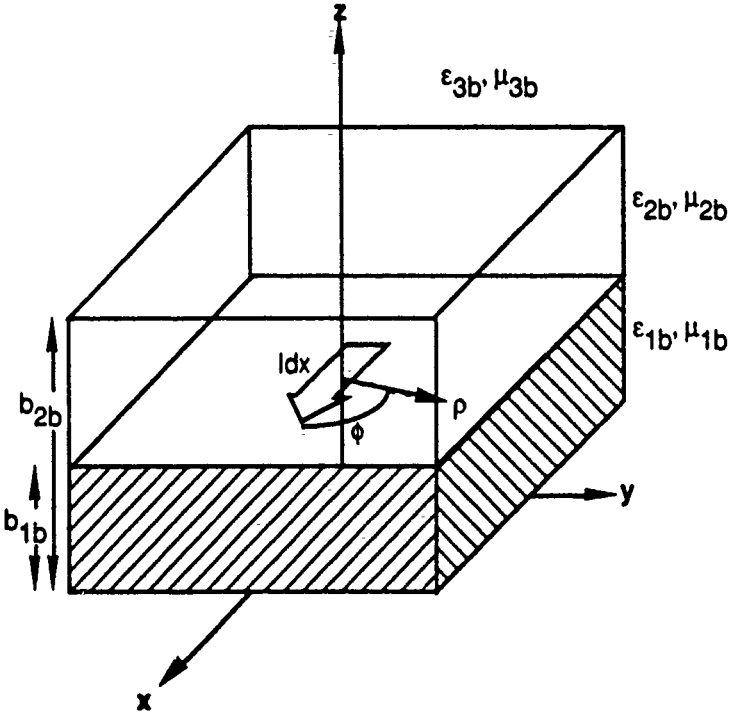

Figure 6. HED at Interface 2b (dielectric 2b is transparent for clarity) [3].

in each dielectric and free space can be expressed in the form of Sommerfeld integrals [17]

$$A^b_{x12}(\rho) = \int_c H_0^{(2)}(\lambda\rho) a^b_{x2} \sinh(u_{1b}z) d\lambda \tag{11}$$

$$A^b_{z12}(\rho) = \cos\phi \int_c H_1^{(2)}(\lambda\rho) a^b_{z2} \cosh(u_{1b}z) d\lambda \tag{12}$$

$$A^b_{x22}(\rho) = \int_c H_0^{(2)}(\lambda\rho)\left[b^b_{x2}\sinh(u_{2b}z) + c^b_{x2}\sinh(u_{2b}z)\right]d\lambda \quad (13)$$

$$A^b_{z22}(\rho) = \cos\phi\int_c H_1^{(2)}(\lambda\rho)\left[b^b_{z2}\sinh(u_{2b}z) + c^b_{z2}\sinh(u_{2b}z)\right]d\lambda \quad (14)$$

$$A^b_{x32}(\rho) = \int_c H_0^{(2)}(\lambda\rho)d^b_{x2}\exp(-u_{3b}z)d\lambda \quad (15)$$

$$A^b_{z32}(\rho) = \cos\phi\int_c H_1^{(2)}(\lambda\rho)d^b_{z2}\exp(-u_{3b}z)d\lambda \quad (16)$$

where a^b_{x2}, a^b_{z2}, b^b_{x2}, etc. are unknown coefficients to be solved for, ρ is the radial distance $|\rho|$ between the source HED and the observer point and

$$u_{1b} = \sqrt{\lambda^2 - k^2_{1b}}, \quad u_{2b} = \sqrt{\lambda^2 - k^2_{2b}}, \quad u_{3b} = \sqrt{\lambda^2 - k^2_{3b}}$$

with k_{1b}, k_{2b}, and k_{3b} being the wave numbers in dielectrics 1b, 2b , and 3b, respectively. Although k_{3b} is assumed to be the free space value, k_0, it is referred to as k_{3b} for notation consistency. The wave numbers are defined as

$$k_{1b} = \omega\sqrt{\varepsilon_{1b}\mu_{1b}}, \quad k_{2b} = \omega\sqrt{\varepsilon_{2b}\mu_{2b}}, \quad k_{3b} = \omega\sqrt{\varepsilon_{3b}\mu_{3b}}$$

with $\varepsilon_{1b,2b,3b}$ and $\mu_{1b,2b,3b}$ being the permittivities and permeabilities of the corresponding medium. As an example of the notation, A^b_{x12} is defined as the x-directed magnetic vector potential in region b, dielectric 1b ($0 \le z \le b_{1b}$) for a HED at interface 2b. The remaining vector potentials, $A^b_{x,z,nm}$ are defined similarly. A definition of the integration path C along with some background of the development of Eqs (11) - (16) can be found in the works by Nazar [3], and Mosig and Gardiol [17].

Nazar developed the necessary boundary condition to solve for the coefficients of Eqs (11) - (16). The relevant results applicable to this work are summarized as follows:

@ $z = b_{1b}$

$$A^b_{z12} = A^b_{x22} \quad (17)$$

$$\frac{1}{\mu_{1b}}\frac{\partial A^b_{x12}}{\partial z} - \frac{1}{\mu_{2b}}\frac{\partial A^b_{x22}}{\partial z} = \frac{\delta(\rho)}{2\pi\rho} \tag{18}$$

$$\frac{A^b_{z12}}{\mu_{1b}} = \frac{A^b_{z22}}{\mu_{2b}} \tag{19}$$

$$\frac{1}{\varepsilon_{1b}\mu_{1b}}\frac{\partial A^b_{z12}}{\partial z} - \frac{1}{\varepsilon_{2b}\mu_{2b}}\frac{\partial A^b_{z22}}{\partial z} = \cos\phi\left(\frac{1}{\varepsilon_{2b}\mu_{2b}} - \frac{1}{\varepsilon_{1b}\mu_{1b}}\right)\frac{\partial A^b_{x12}}{\partial \rho} \tag{20}$$

@ $z = b_{2b}$

$$A^b_{x22} = A^b_{x32} \tag{21}$$

$$\frac{1}{\mu_{2b}}\frac{\partial A^b_{x22}}{\partial z} = \frac{1}{\mu_{3b}}\frac{\partial A^b_{x32}}{\partial z} \tag{22}$$

$$\frac{A^b_{z22}}{\mu_{2b}} = \frac{A^b_{z32}}{\mu_{3b}} \tag{23}$$

$$\frac{1}{\varepsilon_{2b}\mu_{2b}}\frac{\partial A^b_{z22}}{\partial z} - \frac{1}{\varepsilon_{3b}\mu_{3b}}\frac{\partial A^b_{z32}}{\partial z} = \cos\phi\left(\frac{1}{\varepsilon_{3b}\mu_{3b}} - \frac{1}{\varepsilon_{2b}\mu_{2b}}\right)\frac{\partial A^b_{x32}}{\partial \rho} \tag{24}$$

along with the Sommerfeld radiation condition

$$\lim_{r\to\infty} r\left(\frac{\partial \mathbf{A}}{\partial r} + jk\mathbf{A}\right) = 0 \tag{25}$$

where $\mathbf{A}$ satisfies the homogenous Helmholtz equation

$$\left(\nabla^2 + k^2\right)\mathbf{A} = 0 \tag{26}$$

The branch interpretation [18] of $u_{3b} = \sqrt{\lambda^2 - k^2_{3b}}$ is determined by the Sommerfeld radiation condition as

$$u_{3b} = \left|\sqrt{\lambda^2 - k^2_{3b}}\right|, \quad |\lambda| \geq k_{3b}$$

$$u_{3b} = j\left|\sqrt{\lambda^2 - k^2_{3b}}\right|, \quad |\lambda| \leq k_{3b}$$

The term $\delta(\rho)/(2\pi\rho)$ in equation (18) represents a unit current source ($Idx = 1$ A m) on interface 1b, where $\delta(\rho)$ is the Dirac delta function which can be expressed as [17]

$$\delta(\rho) = \frac{\rho}{2}\int_c H_0^{(2)}(\lambda\rho)d\lambda \tag{27}$$

Using the boundary conditions defined and Eqs (11) - (16), eight equations are formed and solved for the unknown coefficients [3] yielding

$$A^b_{x12}(\rho) = \frac{1}{4\pi}\int_c H_0^{(2)}(\lambda\rho)\frac{N^b_{ax2}(\lambda)}{D^b_e(\lambda)}\sinh(u_{1b}z)d\lambda \tag{28}$$

$$A^b_{z12}(\rho) = \frac{\cos\phi}{4\pi}\int_c H_1^{(2)}(\lambda\rho)\frac{N^b_{az2}(\lambda)}{D^b_e(\lambda)D^b_m(\lambda)}\cosh(u_{1b}z)d\lambda \tag{29}$$

$$A^b_{x22}(\rho) = \frac{1}{4\pi}\int_c H_0^{(2)}(\lambda\rho)\left[\frac{N^b_{bx2}(\lambda)\sinh(u_{2b}z) + N^b_{cx2}(\lambda)\sinh(u_{2b}z)}{D^b_e(\lambda)}\right]d\lambda \tag{30}$$

$$A^b_{z22}(\rho) = \frac{\cos\phi}{4\pi}\int_c H_1^{(2)}(\lambda\rho)\left[\frac{N^b_{bz2}(\lambda)\sinh(u_{2b}z) + N^b_{cz2}(\lambda)\sinh(u_{2b}z)}{D^b_e(\lambda)D^b_m(\lambda)}\right]d\lambda \tag{31}$$

$$A^b_{x32}(\rho) = \frac{1}{4\pi}\int_c H_0^{(2)}(\lambda\rho)\frac{N^b_{dx2}(\lambda)}{D^b_e(\lambda)}\exp(-u_{3b}z)d\lambda \tag{32}$$

$$A^b_{z32}(\rho) = \frac{\cos\phi}{4\pi}\int_c H_1^{(2)}(\lambda\rho)\frac{N^b_{dz2}(\lambda)}{D^b_e(\lambda)D^b_m(\lambda)}\exp(-u_{3b}z)d\lambda \tag{33}$$

with the N's representing the numerators of $a^b_{x2}, a^b_{z2}, b^b_{x2}, b^b_{z2}$, etc. and D's represent the denominators. The zeros of

$$\begin{aligned} D^b_e(\lambda) = {} & [\mu_{b12}u_{3b} + u_{1b}\coth(b_{1b}u_{1b})]\,u_{2b}\cosh(u_{2b}(b_{2b} - b_{1b})) \\ & + [\mu_{b12}u^2_{2b} + \mu_{b23}u_{1b}u_{3b}\cot(b_{1b}u_{1b})]\sinh(u_{2b}(b_{2b} - b_{1b})) \end{aligned} \tag{34}$$

$$\begin{aligned} D^b_m(\lambda) = {} & [\varepsilon_{b13}u_{3b} + u_{1b}\tanh(b_{1b}u_{1b})]\,u_{2b}\cosh(u_{2b}(b_{2b} - b_{1b})) \\ & + [\varepsilon_{b12}u^2_{2b} + \varepsilon_{b23}u_{1b}u_{3b}\tan(b_{1b}u_{1b})]\sinh(u_{2b}(b_{2b} - b_{1b})) \end{aligned} \tag{35}$$

define the surface wave poles in the dielectrics where

$$\varepsilon_{b12} = \frac{\varepsilon_{1b}}{\varepsilon_{2b}}, \quad \varepsilon_{b23} = \frac{\varepsilon_{2b}}{\varepsilon_{3b}}, \quad \varepsilon_{b13} = \frac{\varepsilon_{1b}}{\varepsilon_{3b}}$$

and

$$\mu_{b12} = \frac{\mu_{1b}}{\mu_{2b}}, \quad \mu_{b23} = \frac{\mu_{2b}}{\mu_{3b}}, \quad \mu_{b13} = \frac{\mu_{1b}}{\mu_{3b}}$$

The frequencies at which the TE and TM surface waves propagate are determined by the roots of $D_e^b(\lambda)$ and $D_m^b(\lambda)$ [3]. The surface waves represent power propagating along the surface of the dielectric layers, instead of radiating into space. $D_e^b(\lambda)$ and $D_m^b(\lambda)$ are related to the reflection factors on a microstrip structure for an incident perpendicular polarized wave (TE) and parallel polarized wave (TM), respectively [17]. The N terms are given in Appendix A.

3.2.2 HED at Interface 3b [3]. The case for a HED located on the dielectric 2b and dielectric 3b (free space) is shown in Figure 7.

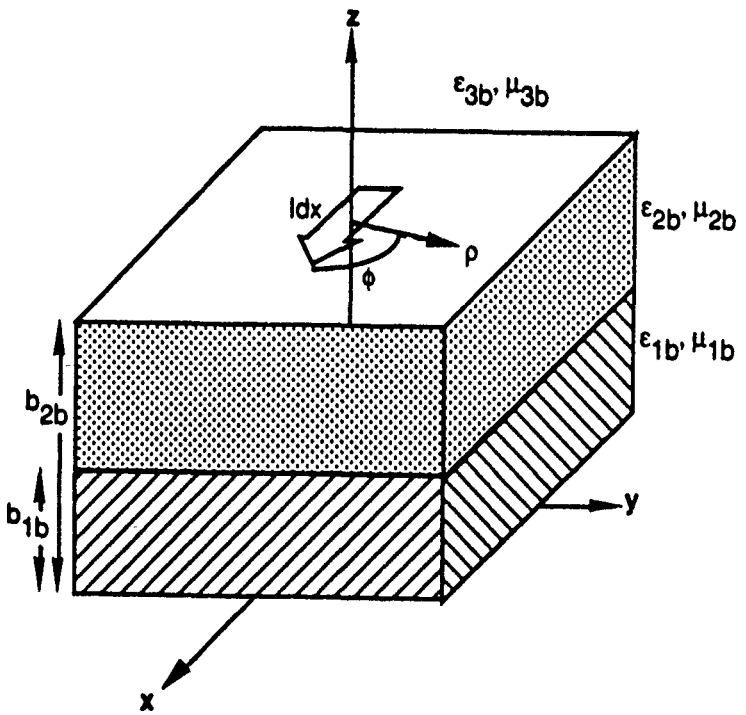

Figure 7. HED at Interface 3b [3].

The x and z components of the magnetic vector potential in each dielectric and free space [3] can be expressed as

$$A^b_{x13}(\rho) = \int_c H_0^{(2)}(\lambda\rho) a^b_{x3} \sinh(u_{1b}z) d\lambda \tag{36}$$

$$A^b_{z13}(\rho) = \cos\phi \int_c H_1^{(2)}(\lambda\rho) a^b_{z3} \cosh(u_{1b}z) d\lambda \tag{37}$$

$$A^b_{x23}(\rho) = \int_c H_0^{(2)}(\lambda\rho) \left[b^b_{x3} \sinh(u_{2b}z) + c^b_{x3} \sinh(u_{2b}z)\right] d\lambda \tag{38}$$

$$A^b_{z23}(\rho) = \cos\phi \int_c H_1^{(2)}(\lambda\rho) \left[b^b_{z3} \sinh(u_{2b}z) + c^b_{z3} \sinh(u_{2b}z)\right] d\lambda \tag{39}$$

$$A^b_{x33}(\rho) = \int_c H_0^{(2)}(\lambda\rho) d^b_{x3} \exp(-u_{3b}z) d\lambda \tag{40}$$

$$A^b_{z33}(\rho) = \cos\phi \int_c H_1^{(2)}(\lambda\rho) d^b_{z3} \exp(-u_{3b}z) d\lambda \tag{41}$$

The boundary conditions needed to solve for the coefficients of equations (36) - (41) are:

@ $z = b_{1b}$

$$A^b_{x13} = A^b_{x23} \tag{42}$$

$$\frac{1}{\mu_{1b}} \frac{\partial A^b_{x13}}{\partial z} = \frac{1}{\mu_{2b}} \frac{\partial A^b_{x23}}{\partial z} \tag{43}$$

$$\frac{A^b_{z13}}{\mu_{1b}} = \frac{A^b_{z23}}{\mu_{2b}} \tag{44}$$

$$\frac{1}{\varepsilon_{1b}\mu_{1b}} \frac{\partial A^b_{z13}}{\partial z} - \frac{1}{\varepsilon_{2b}\mu_{2b}} \frac{\partial A^b_{z23}}{\partial z} = \cos\phi \left(\frac{1}{\varepsilon_{2b}\mu_{2b}} - \frac{1}{\varepsilon_{1b}\mu_{1b}}\right) \frac{\partial A^b_{x13}}{\partial \rho} \tag{45}$$

@ $z = b_{2b}$

$$A^b_{x23} = A^b_{x33} \tag{46}$$

$$\frac{1}{\mu_{2b}} \frac{\partial A^b_{x23}}{\partial z} - \frac{1}{\mu_{3b}} \frac{\partial A^b_{x33}}{\partial z} = \frac{\delta(\rho)}{2\pi\rho} \tag{47}$$

$$\frac{A^b_{z23}}{\mu_{2b}} = \frac{A^b_{z33}}{\mu_{3b}} \tag{48}$$

$$\frac{1}{\varepsilon_{2b}\mu_{2b}} \frac{\partial A^b_{z23}}{\partial z} - \frac{1}{\varepsilon_{3b}\mu_{3b}} \frac{\partial A^b_{z33}}{\partial z} = \cos\phi \left(\frac{1}{\varepsilon_{3b}\mu_{3b}} - \frac{1}{\varepsilon_{2b}\mu_{2b}}\right) \frac{\partial A^b_{x33}}{\partial \rho} \tag{49}$$

along with the Sommerfeld radiation condition of Eq (25). As before, the term $\delta(\rho)/2\pi\rho$ in Eq (47) represents a unit current source, but this time on interface 2b. Solving for the unknown coefficients results in the following

$$A^b_{x13}(\rho) = \frac{1}{4\pi}\int_c H_0^{(2)}(\lambda\rho)\frac{N^b_{ax3}(\lambda)}{D^b_e(\lambda)}\sinh(u_{1b}z)d\lambda \tag{50}$$

$$A^b_{z13}(\rho) = \frac{\cos\phi}{4\pi}\int_c H_1^{(2)}(\lambda\rho)\frac{N^b_{az3}(\lambda)}{D^b_e(\lambda)D^b_m(\lambda)}\cosh(u_{1b}z)d\lambda \tag{51}$$

$$A^b_{x23}(\rho) = \frac{1}{4\pi}\int_c H_0^{(2)}(\lambda\rho)\left[\frac{N^b_{bx3}(\lambda)\sinh(u_{2b}z)+N^b_{cx3}(\lambda)\sinh(u_{2b}z)}{D^b_e(\lambda)}\right]d\lambda \tag{52}$$

$$A^b_{z23}(\rho) = \frac{\cos\phi}{4\pi}\int_c H_1^{(2)}(\lambda\rho)\left[\frac{N^b_{bz3}(\lambda)\sinh(u_{2b}z)+N^b_{cz3}(\lambda)\sinh(u_{2b}z)}{D^b_e(\lambda)D^b_m(\lambda)}\right]d\lambda \tag{53}$$

$$A^b_{x33}(\rho) = \frac{1}{4\pi}\int_c H_0^{(2)}(\lambda\rho)\frac{N^b_{dx3}(\lambda)}{D^b_e(\lambda)}\exp(-u_{3b}z)d\lambda \tag{54}$$

$$A^b_{z33}(\rho) = \frac{\cos\phi}{4\pi}\int_c H_1^{(2)}(\lambda\rho)\frac{N^b_{dz3}(\lambda)}{D^b_e(\lambda)D^b_m(\lambda)}\exp(-u_{3b}z)d\lambda \tag{55}$$

The N terms of equations (50) - (55) are included in Appendix A.

3.2.3 HMD at Interface 1b [3]. The electric fields in region b due to the equivalent magnetic current on the ground plane (see Figure 8) are found with Eq (9) along with Eq (6). The first step in the analysis is to find the fields created by a HMD along the x-axis at the ground plane with a unit moment $Vdx = 1$ V m. Using the same procedure as for the electric sources, the x and z components of the electric vector potential in each dielectric and free space of region b are expressed as

$$F^b_{x11}(\rho) = \int_c H_0^{(2)}(\lambda\rho)\left[a^b_{x1}\sinh(u_{1b}z)+e^b_{x1}\cosh(u_{1b}z)\right]d\lambda \tag{56}$$

$$F^b_{z11}(\rho) = \cos\phi\int_c H_1^{(2)}(\lambda\rho)a^b_{az1}\sinh(u_{1b}z)d\lambda \tag{57}$$

$$F^b_{x21}(\rho) = \int_c H_0^{(2)}(\lambda\rho)\left[b^b_{x1}\sinh(u_{2b}z)+c^b_{x1}\cosh(u_{2b}z)\right]d\lambda \tag{58}$$

$$F^b_{z21}(\rho) = \cos\phi\int_c H_1^{(2)}(\lambda\rho)\left[b^b_{z1}\sinh(u_{2b}z)+c^b_{z1}\cosh(u_{2b}z)\right]d\lambda \tag{59}$$

$$F^b_{x31}(\rho) = \int_c H_0^{(2)}(\lambda\rho)d^b_{x1}\exp(-u_{3b}z)d\lambda \tag{60}$$

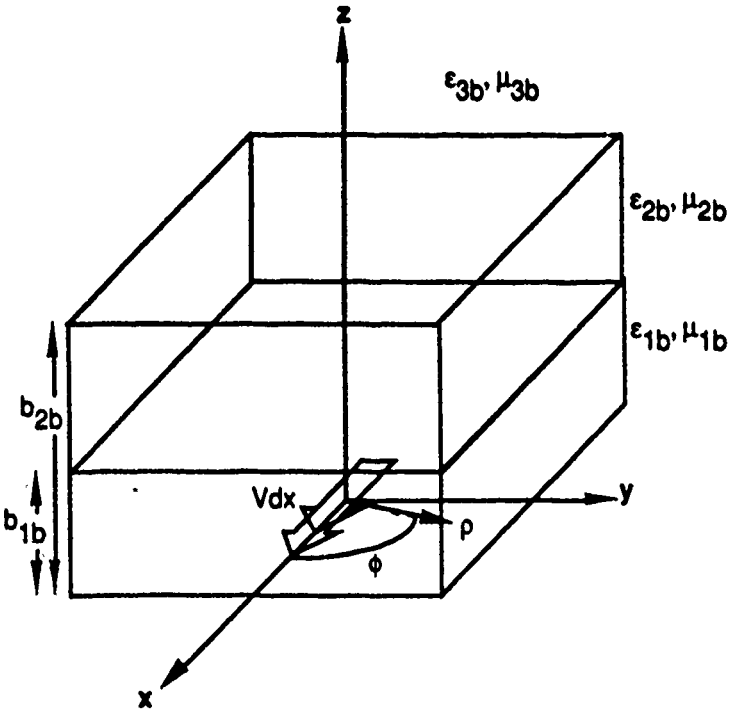

Figure 8. HMD at Interface 1b (dielectrics 1b & 2b are transparent for clarity) [3].

$$F^b_{z31}(\rho) = \cos\phi \int_c H_1^{(2)}(\lambda\rho) d^b_{z1} \exp(-u_{3b}z) d\lambda \tag{61}$$

The boundary conditions needed to solve for the unknown coefficients are:

@ z = 0

$$\frac{1}{\varepsilon_{1b}} \frac{\partial F^b_{x11}}{\partial z} = -\frac{\delta(\rho)}{2\pi\rho} \tag{62}$$

@ z = b_{1b}

$$F^b_{x11} = F^b_{x2} \tag{63}$$

$$\frac{1}{\varepsilon_{1b}} \frac{\partial F^b_{x11}}{\partial z} = \frac{1}{\varepsilon_{2b}} \frac{\partial F^b_{x21}}{\partial z} \tag{64}$$

$$\frac{F^b_{z11}}{\varepsilon_{1b}} = \frac{F^b_{z21}}{\varepsilon_{2b}} \tag{65}$$

$$\frac{1}{\varepsilon_{1b}\mu_{1b}} \frac{\partial F^b_{z11}}{\partial z} - \frac{1}{\varepsilon_{2b}\mu_{2b}} \frac{\partial F^b_{z21}}{\partial z} = \cos\phi \left(\frac{1}{\varepsilon_{2b}\mu_{2b}} - \frac{1}{\varepsilon_{1b}\mu_{1b}} \right) \frac{\partial F^b_{x11}}{\partial \rho} \tag{66}$$

@ $z = b_{2b}$

$$F^b_{x21} = F^b_{x31} \tag{67}$$

$$\frac{1}{\epsilon_{2b}}\frac{\partial F^b_{x21}}{\partial z} = \frac{1}{\epsilon_{3b}}\frac{\partial F^b_{x31}}{\partial z} \tag{68}$$

$$\frac{F^b_{z21}}{\epsilon_{2b}} = \frac{F^b_{z31}}{\epsilon_{3b}} \tag{69}$$

$$\frac{1}{\epsilon_{2b}\mu_{2b}}\frac{\partial F^b_{z21}}{\partial z} - \frac{1}{\epsilon_{3b}\mu_{3b}}\frac{\partial F^b_{z31}}{\partial z} = \cos\phi\left(\frac{1}{\epsilon_{3b}\mu_{3b}} - \frac{1}{\epsilon_{2b}\mu_{2b}}\right)\frac{\partial F^b_{x31}}{\partial \rho} \tag{70}$$

along with the Sommerfeld radiation condition, Eq (25), with **A** replaced with **F**. As before, the term $-\delta(\rho)/(2\pi\rho)$ in Eq (62) represents the unit magnetic current source on the ground plane (interface 1b). The solutions of Eqs (56)-(61) are as follows

$$F^b_{x11}(\rho) = \frac{1}{4\pi}\int_c H^{(2)}_0(\lambda\rho)\left[-\frac{\epsilon_{1b}\lambda}{u_{1b}}\sinh(u_{1b}z) + \frac{N^b_{ex1}(\lambda)\cosh(u_{1b}z)}{u_{1b}D^b_m(\lambda)}\right]d\lambda \tag{71}$$

$$F^b_{z11}(\rho) = \frac{\cos\phi}{4\pi}\int_c H^{(2)}_1(\lambda\rho)\frac{N^b_{az1}(\lambda)}{D^b_e(\lambda)D^b_m(\lambda)}\sinh(u_{1b}z)d\lambda \tag{72}$$

$$F^b_{x21}(\rho) = \frac{1}{4\pi}\int_c H^{(2)}_0(\lambda\rho)\frac{[N^b_{bx1}(\lambda)\sinh(u_{2b}z) + N^b_{cx1}(\lambda)\cosh(u_{2b}z)]}{D^b_m(\lambda)}d\lambda \tag{73}$$

$$F^b_{z21}(\rho) = \frac{\cos\phi}{4\pi}\int_c H^{(2)}_1(\lambda\rho)\left[\frac{N^b_{bz1}(\lambda)\sinh(u_{2b}z) + N^b_{cz1}(\lambda)\cosh(u_{2b}z)}{D^b_e(\lambda)D^b_m(\lambda)}\right]d\lambda \tag{74}$$

$$F^b_{x31}(\rho) = \frac{1}{4\pi}\int_c H^{(2)}_0(\lambda\rho)\frac{N^b_{dx1}(\lambda)}{D^b_m(\lambda)}\exp(-u_{3b}z)d\lambda \tag{75}$$

$$F^b_{z31}(\rho) = \frac{\cos\phi}{4\pi}\int_c H^{(2)}_1(\lambda\rho)\frac{N^b_{dz1}(\lambda)}{D^b_e(\lambda)D^b_m(\lambda)}\exp(-u_{3b}z)d\lambda \tag{76}$$

The numerator terms are listed in Appendix A.

3.2.4 The Electric Scalar Potential [3]. To determine the electric field of Eq (5) the electric scalar potentials are needed. The potentials can be found using the Lorentz gauge condition for electric sources:

$$\nabla \cdot \mathbf{A} + j\omega\epsilon\mu V = 0 \tag{77}$$

When applied to the magnetic vector potentials previously calculated, Eq (77) will yield the potentials for two opposite electric point charges. To determine the Green's functions of Eq (8), the potentials of a single point charge are needed. The electric potential, V_q, of a single point charge can be found using the electrostatic relationship linking an electric point charge and a dipole potential [17]:

$$V = -\frac{\partial V_q}{\partial x} \tag{78}$$

V_q can be found within an arbitrary constant by integrating V over x. The value of the constant is unimportant since the gradient of V_q is taken to calculate the electric field.

3.2.4.1 Scaler Potential for HED at Interface 2b [3]. Applying Eq (77) to Eqs (28) and (29) yields

$$j\omega\varepsilon_{1b}\mu_{1b}V^b_{12} = -\left[\frac{\partial A^b_{x12}}{\partial x} + \frac{\partial A^b_{z12}}{\partial z}\right] \tag{79}$$

resulting in

$$V^b_{12}(\rho) = \frac{\cos\phi}{4\pi j\omega\varepsilon_{1b}\mu_{1b}}\int_c H^{(2)}_1\left[\lambda\frac{N^b_{ax2}(\lambda)}{D^b_e(\lambda)} - u_{1b}\frac{N^b_{az2}(\lambda)}{D^b_e(\lambda)D^b_m(\lambda)}\right]\sinh(u_{1b}z)d\lambda \tag{80}$$

As previously stated, this potential is for two point charges. Applying Eq (78) to Eq (80) results in

$$V^b_{q12}(\rho) = \frac{1}{4\pi j\omega\varepsilon_{1b}\mu_{1b}}\int_c H^{(2)}_0\left[\frac{N^b_{ax2}(\lambda)}{D^b_e(\lambda)} - \frac{u_{1b}}{\lambda}\frac{N^b_{az2}(\lambda)}{D^b_e(\lambda)D^b_m(\lambda)}\right]\sinh(u_{1b}z)d\lambda \tag{81}$$

The potentials in the other mediums can be found similarly:

$$V^b_{q22}(\rho) = \frac{1}{4\pi j\omega\varepsilon_{2b}\mu_{2b}}\int_c H^{(2)}_0(\lambda\rho)\left\{\begin{array}{l}\left[\frac{N^b_{bx2}(\lambda)}{D^b_e(\lambda)} - \frac{u_{2b}}{\lambda}\frac{N^b_{cz2}(\lambda)}{D^b_e(\lambda)D^b_m(\lambda)}\right]\sinh(u_{2b}z)\\ +\left[\frac{N^b_{cx2}(\lambda)}{D^b_e(\lambda)} - \frac{u_{2b}}{\lambda}\frac{N^b_{bz2}(\lambda)}{D^b_e(\lambda)D^b_m(\lambda)}\right]\cosh(u_{2b}z)\end{array}\right\}d\lambda \tag{82}$$

$$V^b_{q32}(\rho) = \frac{1}{4\pi j\omega\varepsilon_{3b}\mu_{3b}}\int_c H^{(2)}_0(\lambda\rho)\left[\frac{N^b_{dx2}(\lambda)}{D^b_e(\lambda)} - \frac{u_{3b}}{\lambda}\frac{N^b_{dz2}(\lambda)}{D^b_e(\lambda)D^b_m(\lambda)}\right]\exp(-u_{3b}z)d\lambda \tag{83}$$

3.2.4.2 Scalar Potentials for HED at Interface 3b.

$$V^b_{q13}(\rho) = \frac{1}{4\pi j\omega\epsilon_{1b}\mu_{1b}} \int_c H_0^{(2)}(\lambda\rho) \left[\frac{N^b_{ax3}(\lambda)}{D^b_e(\lambda)} - \frac{u_{3b}}{\lambda} \frac{N^b_{az3}(\lambda)}{D^b_e(\lambda) D^b_m(\lambda)} \right] \sinh(u_{1b}z) d\lambda \tag{84}$$

$$V^b_{q23}(\rho) = \frac{1}{4\pi j\omega\epsilon_{2b}\mu_{2b}} \int_c H_0^{(2)}(\lambda\rho) \left\{ \begin{array}{l} \left[\frac{N^b_{bx3}(\lambda)}{D^b_e(\lambda)} - \frac{u_{2b}}{\lambda} \frac{N^b_{cz3}(\lambda)}{D^b_e(\lambda) D^b_m(\lambda)} \right] \sinh(u_{2b}z) \\ + \left[\frac{N^b_{cx3}(\lambda)}{D^b_e(\lambda)} - \frac{u_{2b}}{\lambda} \frac{N^b_{bz3}(\lambda)}{D^b_e(\lambda) D^b_m(\lambda)} \right] \cosh(u_{2b}z) \end{array} \right\} d\lambda \tag{85}$$

$$V^b_{q33}(\rho) = \frac{1}{4\pi j\omega\epsilon_{3b}\mu_{3b}} \int_c H_0^{(2)}(\lambda\rho) \left[\frac{N^b_{dx3}(\lambda)}{D^b_e(\lambda)} - \frac{u_{2b}}{\lambda} \frac{N^b_{dz3}(\lambda)}{D^b_e(\lambda) D^b_m(\lambda)} \right] \exp(-u_{3b}z) d\lambda \tag{86}$$

3.3 Green's Functions Construction

The electric fields in any medium may be found using Eqs (5) and (6) along with the vector potentials and the electric scalar potentials. However, only the tangential eclectic fields listed in Table 2 are needed for this analysis.

Table 2. Necessary Tangential Fields [3]

HED at interface 2b (Patch 1):	HMD at interface 1b (Aperture):
1) $\mathbf{E}^{tan}$ at interface 2	1) $\mathbf{E}^{tan}$ at interface 2
2) $\mathbf{E}^{tan}$ at interface 3	2) $\mathbf{E}^{tan}$ at interface 3
HED at interface 3b (Patch 2):	
1) $\mathbf{E}^{tan}$ at interface 2	
2) $\mathbf{E}^{tan}$ at interface 3	

3.3.1 **E** *Fields Due to Electric Sources [3].* Equation (5) is used to calculate the **E** fields due to electric sources. The Green's functions for the case of an electric source on interface 3b and an observer on interface 2b are used to demonstrate the form of the equations.

The tangential **E** field at interface 2b is found by putting equations (52) and (85) into equation (5), yielding

$$\mathbf{E}_{23}^{btan} = \left[-j\omega\left(A_{x23}^{b}\bar{x} + A_{y23}^{b}\bar{y}\right) - \nabla^{t}V_{q32}^{b}\right]_{(z=b_{1b})} \tag{87}$$

where A_{y23}^{b} is the magnetic vector potential for a y-directed current source and is equal to Eq (52). Since only a unit point source located a $\rho = 0$ is assumed initially, the integrals of Eqs (7) and (8) over the point source results in

$$G_{A22}^{bxx}(\rho) = A_{x23}^{b}(\rho) \tag{88}$$

$$G_{A23}^{byy}(\rho) = A_{y23}^{b}(\rho) \tag{89}$$

$$G_{q23}^{b}(\rho) = V_{q23}^{b}(\rho) \tag{90}$$

where $G_{A23}^{bxx}(\rho)$ is defined as the magnetic vector potential in the x-direction (first x in the superscript) on interface 2b for an infinitesimal x-directed current source (second x in the superscript) on interface 3b, with an observer at radial position ρ. The Green's functions in Eqs (89) and (90) are similarly defined. By taking the transverse gradient in cylindrical coordinates and using the identity $\bar{\rho} = \bar{x}\cos\phi + \bar{y}\sin\phi$, Eq (87) becomes

$$\mathbf{E}_{23}^{tan}(\rho) = \left[-j\omega G_{A23}^{bxx}(\rho) - \frac{\partial G_{q23}^{b}(\rho)}{\partial\rho}\cos\phi\right]\bar{x} + \left[-j\omega G_{A23}^{byy}(\rho) - \frac{\partial G_{q23}^{b}(\rho)}{\partial\rho}\sin\phi\right]\bar{y} \tag{91}$$

The Green's functions only depend on the radial separation $\rho = |\rho|$ between the source and observer and not the relative angular position. Equation (91) gives the expression for the tangential **E** field anywhere on interface 2b for a point source at $\rho = 0$ on interface 3b. For generalized source and observer points ($\rho \neq 0$), ρ and ϕ become R and ζ (see Figure 9)

$$\begin{aligned} R &= |\rho - \rho'| \\ \zeta &= \sin^{-1}\left[\frac{\rho\sin\phi - \rho'\sin\phi}{R}\right] \end{aligned} \tag{92}$$

Then for the generalized case for a distribution of sources over interface 3b, Eq (91) becomes

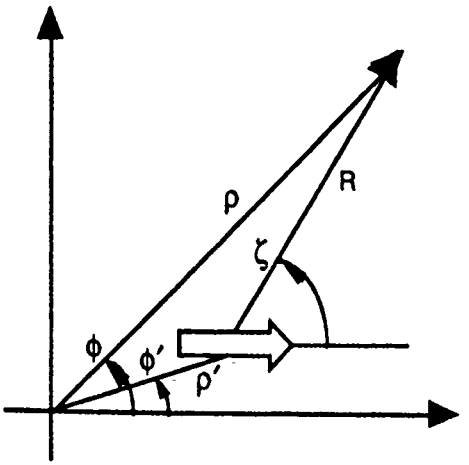

Figure 9. Geometrical Relationships for x-Directed HED at Arbitrary ρ' [3, 17].

$$\mathbf{E}_{23}^{btan}(\rho) = \begin{array}{l} \left[-j\omega \int_{s'} G_{A23}^{bxx}(R) J_{x2}(\rho')ds' - \cos\zeta \int_{s'} G_{q'23}^{b}(R) q_2(\rho')ds'\right] \bar{x} \\ + \left[-j\omega \int_{s'} G_{A23}^{byy}(R) J_{y2}(\rho')ds' - \sin\zeta \int_{s'} G_{q'23}^{b}(R) q_2(\rho')ds'\right] \bar{y} \end{array} \tag{93}$$

where

$$G_{q'23}^{b}(R) = \frac{\partial G_{q23}^{b}(R)}{\partial R}$$

By properly interchanging the Green's functions and source terms in Eq (93), all the tangential **E** fields produced by the HEDs listed in Table 2 can be found. It appears that Nazar inadvertently left out a factor of $j\omega$ from the denominator terms of $G_{q22}^{b}(R), G_{q23}^{b}(R), G_{q33}^{b}(R)$, and $G_{q32}^{b}(R)$. A complete list of all Green's functions can be found in Appendix B.

3.3.2 **E** *Fields Due to Magnetic Sources [3].* The tangential **E** fields at the dielectric interfaces due to the magnetic source on the ground plane are found with Eq (6). An example of calculating one of those fields will be presented.

The tangential **E** field at interface 3b due to an infinitesimal, x-directed magnetic current source on interface 1b (ground plane) can be found by expressing F^b_{31} in cylindrical coordinates

$$F^b_{\rho 31}(\rho) = \frac{\cos\phi}{4\pi}\int_c H_0^{(2)}(\lambda\rho)\frac{N^b_{dx1}(\lambda)}{D^b_m(\lambda)}\exp(-u_{3b}z)d\lambda \quad (94)$$

$$F^b_{\phi 31}(\rho) = \frac{-\sin\phi}{4\pi}\int_c H_0^{(2)}(\lambda\rho)\frac{N^b_{dx1}(\lambda)}{D^b_m(\lambda)}\exp(-u_{3b}z)d\lambda \quad (95)$$

$$F^b_{z31}(\rho) = \frac{\cos\phi}{4\pi}\int_c H_1^{(2)}(\lambda\rho)\frac{N^b_{dz1}(\lambda)}{D^b_e(\lambda)D^b_m(\lambda)}\exp(-u_{3b}z)d\lambda \quad (96)$$

and then applying Eq (6) in cylindrical coordinates results in

$$E^{tan}_{31}(\rho) = -\frac{1}{\varepsilon_{3b}}\left[\left(\frac{1}{\rho}\frac{\partial F^b_{z31}}{\partial\phi} - \frac{\partial F^b_{\phi 31}}{\partial z}\right)\overline{\rho} + \left(\frac{\partial F^b_{\rho 31}}{\partial z} - \frac{\partial F^b_{z31}}{\partial\rho}\right)\overline{\phi}\right]_{(z=b_{1b})} \quad (97)$$

The x and y components of the **E** field can be determined by using $\overline{\rho} = \overline{x}\cos\phi + \overline{y}\sin\phi$ and $\overline{\phi} = -\overline{x}\sin\phi + \overline{y}\cos\phi$, resulting in:

$$E^{bxx}_{31}(\rho) = -\frac{\sin 2\phi}{4\pi\varepsilon_{2b}}\left\{\begin{array}{l} +\frac{1}{2}\int_c H_0^{(2)}(\lambda\rho)\lambda\frac{N^b_{dz1}(\lambda)}{D^b_e(\lambda)D^b_m(\lambda)}\exp(-u_{3b}b_{2b})d\lambda \\ -\frac{1}{\rho}\int_c H_1^{(2)}(\lambda\rho)\frac{N^b_{dz1}(\lambda)}{D^b_e(\lambda)D^b_m(\lambda)}\exp(-u_{3b}b_{2b})d\lambda \end{array}\right\} \quad (98)$$

$$E^{byx}_{31}(\rho) = -\frac{1}{4\pi\varepsilon_{2b}}\left\{\begin{array}{c} +\frac{\cos 2\phi}{\rho}\int_c H_1^{(2)}(\lambda\rho)\frac{N^b_{dz1}(\lambda)}{D^b_e(\lambda)D^b_m(\lambda)}\exp(-u_{3b}b_{2b})d\lambda \\ -\int_c H_0^{(2)}(\lambda\rho)u_{3b}\frac{N^b_{dz1}(\lambda)}{D^b_m(\lambda)}\exp(-u_{3b}b_{2b})d\lambda \\ -\cos^2\phi\int_c H_0^{(2)}(\lambda\rho)\lambda\frac{N^b_{dz1}(\lambda)}{D^b_e(\lambda)D^b_m(\lambda)}\exp(-u_{3b}b_{2b})d\lambda \end{array}\right\} \quad (99)$$

where E^{byx}_{31} designates a y-directed electric field for an x-directed magnetic current element. As before, the integrals of Eqs (98) and (99) only depend on the radial distance between the source and observer points. For an arbitrary distribution of x-directed magnetic current elements let ρ and ϕ become R and ζ as related by Eq (92). Then Eqs (98) and (99) become

$$E^{bxx}_{31}(\rho) = -\int_{s'} G^{bxx}_{E31}(R,\zeta)M^b_{x1}(\rho')ds' \quad (100)$$

$$E_{31}^{byx}(\rho) = -\int_{s'} G_{E31}^{byx}(R,\zeta) M_{x1}^{b}(\rho')ds' \tag{101}$$

where -$G_{E31}^{bxx}(R,\zeta)$ equals the right-hand-side of Eq (98) and -$G_{E31}^{byx}(R,\zeta)$ equals the right-hand-side of Eq (99) for arbitrary source and observer locations.

To determine the **E** fields for y-directed magnetic current sources replace ϕ by $\phi - \pi/2$ in Eqs (94) to (96) [3] and repeat the same procedure used to derive Eqs (98) and (99). The x and y components of the **E** fields at interface 3b due to an infinitesimal, y-directed magnetic current source on interface 1b are then

$$E_{31}^{byy}(\rho) = -\frac{\sin 2\phi}{4\pi\varepsilon_{2b}} \left\{ \begin{array}{l} -\frac{1}{2}\int_c H_0^{(2)}(\lambda\rho)\lambda \frac{N_{dz1}^{b}(\lambda)}{D_e^{b}(\lambda)D_m^{b}(\lambda)} \exp(-u_{3b}b_{2b})d\lambda \\ +\frac{1}{\rho}\int_c H_1^{(2)}(\lambda\rho) \frac{N_{dz1}^{b}(\lambda)}{D_e^{b}(\lambda)D_m^{b}(\lambda)} \exp(-u_{3b}b_{2b})d\lambda \end{array} \right\} \tag{102}$$

$$E_{31}^{bxy}(\rho) = -\frac{1}{4\pi\varepsilon_{2b}} \left\{ \begin{array}{l} +\frac{\cos 2\phi}{\rho}\int_c H_1^{(2)}(\lambda\rho) \frac{N_{dz1}^{b}(\lambda)}{D_e^{b}(\lambda)D_m^{b}(\lambda)} \exp(-u_{3b}b_{2b})d\lambda \\ +\int_c H_0^{(2)}(\lambda\rho)u_{3b} \frac{N_{dz1}^{b}(\lambda)}{D_m^{b}(\lambda)} \exp(-u_{3b}b_{2b})d\lambda \\ +\sin^2\phi \int_c H_0^{(2)}(\lambda\rho)\lambda \frac{N_{dz1}^{b}(\lambda)}{D_e^{b}(\lambda)D_m^{b}(\lambda)} \exp(-u_{3b}b_{2b})d\lambda \end{array} \right\} \tag{103}$$

which are similar to Eqs (98) and (99). For an arbitrary distribution of y-directed magnetic current elements, the **E** fields of Eqs (102) and (103) are represented as

$$E_{31}^{byy}(\rho) = -\int_{s'} G_{E31}^{byy}(R,\zeta) M_{x1}^{b}(\rho')ds' \tag{104}$$

$$E_{31}^{bxy}(\rho) = -\int_{s'} G_{E31}^{bxy}(R,\zeta) M_{x1}^{b}(\rho')ds' \tag{105}$$

The tangential **E** fields can be written more compactly as

$$E_{31}^{btan} = -\int_{s'} \overline{\overline{G}}_{E31}^{b}(R,\zeta) \cdot M_{1}^{b}(\rho')ds' \tag{106}$$

where

$$\overline{\overline{G}}^{b}_{E31}(R,\zeta) = \begin{bmatrix} G^{bxx}_{E31}(R,\zeta)\overline{xx} & G^{bxy}_{E31}(R,\zeta)\overline{xy} \\ G^{byx}_{E31}(R,\zeta)\overline{yx} & G^{byy}_{E31}(R,\zeta)\overline{yy} \end{bmatrix} \tag{107}$$

The tangential **E** fields at interface 2b due to the magnetic surface currents on interface 1b can be found by expressing F^{b}_{21} in cylindrical coordinates and repeating the procedure for $z = b_{1b}$ [3] resulting in

$$\mathbf{E}^{btan}_{21} = -\int_{s'} \overline{\overline{G}}^{b}_{E21}(R,\zeta) \cdot \mathbf{M}^{b}_{1}(\rho')ds' \tag{108}$$

The complete set of Green's functions for this analysis are in Appendix B.

3.4 Integral Equations

The expressions for the **E** fields are integral equations involving the derived Green's functions and the unknown current and charge distributions. The unknown distributions on the patches are found by enforcing the boundary conditions of Table 1. To comply with the boundary condition $\mathbf{E}^{tan} = 0$ on patch 1, the sum of the tangential electric fields due to the sources on patch 1, patch 2 and the equivalent sources on the aperture must equal zero. Using the derived Green's functions and Eq (5), this can be expressed as

$$\begin{aligned} -j\omega \int_{P1} \overline{\overline{G}}^{b}_{A22}(\rho|\rho') \cdot \mathbf{J}_2(\rho')ds' \; - \; \nabla^{t} \int_{P1} G^{b}_{q22}(\rho|\rho') q_2(\rho')ds' \\ -j\omega \int_{P2} \overline{\overline{G}}^{b}_{A23}(\rho|\rho') \cdot \mathbf{J}_3(\rho')ds' \; - \; \nabla^{t} \int_{P1} G^{b}_{q23}(\rho|\rho') q_3(\rho')ds' \\ + \int_{Ap} \overline{\overline{G}}^{b}_{E21}(\rho|\rho') \; \cdot \; \mathbf{M}_1(\rho')ds' = 0 \end{aligned} \tag{109}$$

with

$$\overline{\overline{G}}^{b}_{A22}(\rho|\rho') = \begin{bmatrix} G^{bxx}_{A22}(\rho|\rho')\overline{xx} & 0 \\ 0 & G^{byy}_{A22}(\rho|\rho')\overline{yy} \end{bmatrix} \tag{110}$$

$\overline{\overline{G}}^{b}_{A23}(\rho|\rho')$ is similarly defined and $\mathbf{M}_1(\rho')$ is the assumed magnetic current across the aperture. On patch 2

$$
\begin{aligned}
-j\omega \int_{P1} \overline{\overline{G}}^{b}_{A32}(\rho|\rho') \cdot \mathbf{J}_2(\rho')ds' - \nabla^t \int_{P1} G^{b}_{q32}(\rho|\rho')q_2(\rho')ds' \\
-j\omega \int_{P2} \overline{\overline{G}}^{b}_{A33}(\rho|\rho') \cdot \mathbf{J}_3(\rho')ds' - \nabla^t \int_{P1} G^{b}_{q33}(\rho|\rho')q_3(\rho')ds' \\
+ \int_{Ap} \overline{\overline{G}}^{b}_{E31}(\rho|\rho') \cdot \mathbf{M}_1(\rho')ds' = 0
\end{aligned}
\tag{111}
$$

The unknown current and charge distributions in Eqs (109) and (111) can be solved using a method of moments approach which converts the integral equations to matrix equations.

3.5 Approximation Theory

Given a set of discrete values for a function, approximations for intermediate values can be determined by two separate but related processes [19]. If the values are assumed accurate then an interpolation scheme can be used. This involves determining a function whose curve will pass through each data point or a chosen subset of those points. If the discrete data are thought to contain errors then a curve fitting process can be used to try and average out these errors.

The Green's function data to be approximated was assumed accurate, so the first thought might be to use an interpolation technique. The numerical data for each Green's function consisted of 50 data sets which would require an interpolation polynomial of order 49 if all the data sets were used. The process of determining the coefficients of this size polynomial would only be trading one computationally intense process for another. Using only a subset of the data would be possible if one knew a priori which data sets should be used. No previous knowledge of the data to be approximated was assumed, so all the data was used in determining the approximations. Thus to use all the data, a curve fitting method was chosen to determine a polynomial or functional approximation of hopefully much lower order. A linear least squares method was chosen for use in

determining the coefficients of the approximation functions.

In the least squares method a form of function or a polynomial is assumed and the coefficients are solved for based upon the goal of minimizing the square of the error between the original function and the approximation. An outline of the method as presented by Stark [19] follows.

Given a table of $n+1$ points, an approximating function of the form

$$p_m(x) = a_m g_m(x) + a_{m-1} g_{m-1}(x) + \cdots + a_1 g_1(x) + a_0 g_0(x) \tag{112}$$

is assumed, where the functions $g_m(x), \ldots, g_0(x)$ are some known functions of x. The approximating function is sought to match the $n+1$ given points in such a way that if a set of deviations were formed, one for each tabulated x_i,

$$\begin{aligned}
\delta_0 &= p_m(x_0) - f(x_0) \\
\delta_1 &= p_m(x_1) - f(x_1) \\
\delta_2 &= p_m(x_2) - f(x_2) \\
&\vdots \\
\delta_n &= p_m(x_n) - f(x_n)
\end{aligned}$$

or, in general terms, the set of deviations

$$\delta_i = p_m(x_i) - f(x_i) \quad \text{for } i = 0, 1, 2, \ldots, n \tag{113}$$

then the sum of the squares of these $n+1$ deviations should be a minimum:

$$\sum_{i=0}^{n} (\delta_i)^2 = \text{a minimum.} \tag{114}$$

The summation in Eq. (114) can also be written as

$$\sum_{i=0}^{n}(\delta_i)^2 = \sum_{i=0}^{n}[p_m(x_i) - f(x_i)]^2 \tag{115}$$

$$\sum_{i=0}^{n}(\delta_i)^2 = \sum_{i=0}^{n}[a_m g_m(x_i) + \cdots + a_0 g_0(x_i) - f(x_i)]^2 \tag{116}$$

The object is to minimize the right-hand side of Eq. (116). Since the x_i and $f(x_i)$ are given in the original table, and the $g_i(x)$ are known functions which can be evaluated at the given x_i, the only unknowns in Eq. (116) are the coefficients a_i. Thus Eq. (116) can be looked on as a function of the $m+1$ coefficients a_i with all the other terms being known constants.

To minimize a function its first derivative is set equal to zero and the equation is solved for the unknown variable. In this case the function to be minimized, Eq (116), is actually a function of the $m+1$ unknowns a_i. The first step in solving for the unknowns is to find the partial derivative of the summation with respect to *each* of the $m+1$ variables a_i, and set *each* of these derivatives equal to zero:

$$\begin{aligned}
\frac{\partial}{\partial a_0}\sum_{i=0}^{n}(\delta_i)^2 &= 0 \\
\frac{\partial}{\partial a_1}\sum_{i=0}^{n}(\delta_i)^2 &= 0 \\
&\vdots \\
\frac{\partial}{\partial a_m}\sum_{i=0}^{n}(\delta_i)^2 &= 0,
\end{aligned}$$

or, in general terms

$$\frac{\partial}{\partial a_i}\sum_{i=0}^{n}(\delta_i)^2 = 0 \quad \text{for } j = 0, 1, 2, \ldots, m. \tag{117}$$

The series has a finite number of terms, and so the derivative of a sum is equal to the sum of the derivatives of the terms. Thus Eq (117) can be written as

$$\begin{aligned}\frac{\partial}{\partial a_j}\sum_{i=0}^{n}(\delta_i)^2 &= \sum_{i=0}^{n}\frac{\partial}{\partial a_j}(\delta_i)^2 \\ &= \sum_{i=0}^{n}2\delta_i\frac{\partial \delta_i}{\partial a_j} = 0\end{aligned}$$

or,

$$\sum_{i=0}^{n}\delta_i\frac{\partial \delta_i}{\partial a_j} = 0 \quad \text{for } j = 0,1,2,\ldots,m. \tag{118}$$

The differentiation of any δ_i with respect to a_j is simple when noting that

$$\begin{aligned}\delta_i &= p_m(x_i) - f(x_i) \\ &= a_m g_m(x_i) + a_{m-1}g_{m-1}(x_i) + \cdots + a_j g_j(x_i) + \cdots \\ &\quad + a_1 g_1(x_i) + a_0 g_0(x_i) - f(x_i).\end{aligned} \tag{119}$$

When differentiating with respect to a_j, every other term in Eq (119) is assumed constant except the term containing a_j, so that all the other terms drop out upon differentiating, and

$$\begin{aligned}\frac{\partial \delta_i}{\partial a_j} &= 0 + 0 + \cdots + \frac{\partial}{\partial a_j}a_j g_j(x_i) + 0 + \cdots + 0 \\ \frac{\partial \delta_i}{\partial a_j} &= g_j(x_i).\end{aligned} \tag{120}$$

Now substituting Eq (120) into Eq (118), $m+1$ equations are obtained:

$$\sum_{i=0}^{n}\delta_i g_i(x_i) = 0 \quad \text{for } j = 0,1,2,\ldots,m \tag{121}$$

Substituting Eq (113) into Eq (121, results in

$$\sum_{i=0}^{n} [p_m(x_i) - f(x_i)]\, g_j(x_i) = 0 \qquad \text{for } j = 0, 1, 2, \ldots, m, \tag{122}$$

and then substituting Eq (112) into (122) leaves

$$\sum_{i=o}^{n} [a_m g_m(x_i) + \cdots + a_1 g_1(x_i) + a_0 g_0(x_i) - f(x_i)]\, g_j(x_i) = 0$$

$$\text{for } j = 0, 1, 2, \ldots, m \tag{123}$$

Multiplying through on the left-hand side

$$\sum_{i=0}^{n} [a_m g_m(x_i) g_j(x_i) + \cdots + a_1 g_1(x_i) g_j(x_i)$$

$$+ a_0 g_0(x_i) g_j(x_i) - f(x_i) g_j(x_i)] = 0 \qquad \text{for } j = 0, 1, 2, \ldots, m$$

Breaking up the left-hand side into separate sums results in:

$$\sum_{i=0}^{n} a_m g_m(x_i) g_j(x_i) \quad + \quad \cdots + \sum_{i=0}^{n} a_1 g_1(x_i) g_j(x_i)$$

$$+ \quad \sum_{i=0}^{n} a_0 g_0(x_i) g_j(x_i) - \sum_{i=0}^{n} f(x_i) g_j(x_i) = 0$$

$$\text{for } j = 0, 1, 2, \cdots, m$$

Next factor the a's out of each term:

$$a_m \sum_{i=0}^{n} g_m(x_i) g_j(x_i) \quad + \quad \cdots + a_1 \sum_{i=0}^{n} g_1(x_i) g_j(x_i)$$

$$+ \quad a_0 \sum_{i=0}^{n} g_0(x_i) g_j(x_i) = \sum_{i=0}^{n} f(x_i) g_j(x_i) \tag{124}$$

$$\text{for } j = 0, 1, 2, \cdots, m$$

Eq (124) provides a useful result because each of the summations can be evaluated since the g_i's are known functions and the x_i's are tabulated values. Eq (124) is actually a system of $m+1$ linear equations with the a_i's the only unknowns. These linear equations can then be solved by using any of a number of standard methods for the solution of a system of simultaneous linear equations.

To simplify the process a bit and make it more suitable for computer solution it should be noted that the coefficient of a_k in the jth equation is

$$\alpha_{kj} = \sum_{i=0}^{n} g_k(x_i) g_j(x_i) \qquad \begin{matrix} \text{for } k = 0, 1, 2, \ldots, m \\ j = 0, 1, 2, \ldots, m \end{matrix} \tag{125}$$

Since j and k in Eq (125) can be interchanged, $\alpha_{kj} = \alpha_{jk}$, which reduces the work required to compute these coefficients by half.

The method presented provides a workable scheme for finding the least-squares fit. Using Eq (124) the $m + 1$ equations are solved for the unknown a's, which exist and are unique if the $g(x)$ functions are chosen properly. The resulting a's are then substituted into Eq (112) to give the desired expression for $p_m(x)$.

IV. Results

To determine the surface current and charge distribution of the antenna by using the method of moments, an efficient method is needed to numerically evaluate the Green's functions. The Green's functions as developed by Nazar are complex valued integral functions. In his thesis he examined the Green's functions expressions, developed techniques to numerically integrate them, and coded representative examples to show their behavior as a function of the radial separation between the source and observer. This thesis effort concentrated on coding the remaining Green's functions needed and developing approximations that could be used in an efficient moment method analysis of the antenna. All the needed Green's functions were calculated numerically and then various curve fitting schemes were tried until suitable approximations were found for each. The curve fitting was done using a least squares method to test the fit of the various approximations. All the custom written code developed in this thesis was written in FORTRAN.

4.1 Numerical Evaluation of the Green's Functions

Before approximations could be made for the Green's functions, the remaining Green's functions needed to be coded and numerical results obtained. The examples coded by Nazar represented all the unique forms of the Green's functions so his results were extended by coding the remaining Green's function integrands and using the integration routines he developed [3]. A complete list of the Green's functions needed for this model is listed in Table 3. The redundant forms are indicated by their equivalent forms. The Green's functions used to calculate the contribution to the **E** field from the equivalent magnetic sources have an angular as well as a radial dependence. Each of these functions is composed of two or three integral functions which each have only a radial dependence. Table 4 shows which integral equations are the components of these Green's functions. All the approximations in this thesis have only a radial dependence.

Table 3. Green's Functions for Various Source Contributions

HED on Interface 2b	HED on Interface 3b
$G^{bxx}_{A22}(R)$	$G^{bxx}_{A33}(R)$
$G^{byy}_{A22}(R)=G^{bxx}_{A22}(R)$	$G^{byy}_{A33}(R)=G^{bxx}_{A33}(R)$
$G^{b}_{q22}(R)$	$G^{b}_{q33}(R)$
$G^{bxx}_{A32}(R)$	$G^{bxx}_{A23}(R)=G^{bxx}_{A32}(R)$
$G^{byy}_{A32}(R)=G^{bxx}_{A32}(R)$	$G^{byy}_{A23}(R)=G^{bxx}_{A32}(R)$
$G^{b}_{q32}(R)$	$G^{b}_{q23}(R)$
HMD on Interface 1b	
$G^{bxx}_{E21}(R,\zeta)$	$G^{bxx}_{E31}(R,\zeta)$
$G^{byx}_{E21}(R,\zeta)$	$G^{byx}_{E31}(R,\zeta)$
$G^{bxy}_{E21}(R,\zeta)$	$G^{bxy}_{E31}(R,\zeta)$
$G^{byy}_{E21}(R,\zeta)$	$G^{byy}_{E31}(R,\zeta)$

Table 4. Green's Functions Integral Components

HMD on Interface 1b	
$G^{bxx}_{E21}(I^{r}_{b21}(R), I^{s}_{b21}(R))$	$G^{bxx}_{E31}(I^{r}_{b31}(R), I^{s}_{b31}(R))$
$G^{byx}_{E21}(I^{r}_{b21}(R), I^{s}_{b21}(R), I^{t}_{b21}(R))$	$G^{byx}_{E31}(I^{r}_{b31}(R), I^{s}_{b31}(R), I^{t}_{b31}(R))$
$G^{bxy}_{E21}(I^{r}_{b21}(R), I^{s}_{b21}(R), I^{t}_{b21}(R))$	$G^{bxy}_{E31}(I^{r}_{b31}(R), I^{s}_{b31}(R), I^{t}_{b31}(R))$
$G^{byy}_{E21}(I^{r}_{b21}(R), I^{s}_{b21}(R))$	$G^{byy}_{E31}(I^{r}_{b31}(R), I^{s}_{b31}(R))$

4.1.1 Behavior as $R \rightarrow 0$. To determine the currents using the method of moments, it is necessary to perform a surface integration over the source and observer areas [3]. When the source and observer are on separate planes, the Green's functions integrands decay exponentially and the Green's functions can be solved and evaluated for a discrete series of R values between $R = 0$ and the maximum radial separation expected in the antenna design. Once the Green s functions have been evaluated for a discrete number of R values, then a suitable approximation can be made to fit to the data. This approximation would be much more computationally efficient than trying to evaluate the Green's function each time a value is needed. Unfortunately this method fails when the source and observer are on the same plane.

When the source and observer are on the same plane the integrands of the Green's functions do not decay. Nazar developed asymptotic approximations for all the Green's functions where the source and observer are coplanar. For example, the asymptotic approximation for $G_{Axx}^{b22}(r)$ as $R \rightarrow 0$ becomes

$$G_{A22}^{bxx}(R) \approx \frac{\mu_{1b}}{2\pi}\left[\int_0^{\lambda_c} J_0(\lambda R)\lambda \frac{u_{2b}\cosh(u_{2b}(b_{2b}-b_{1b})) + \mu_{b23}u_{3b}\sinh(u_{2b}(b_{2b}-b_{1b}))}{D_e^b(\lambda)}d\lambda \right.$$
$$\left. - \frac{1+\mu_{b23}}{1+\mu_{b12}+\mu_{b23}+\mu_{b13}}\int_0^{R\lambda_c}\frac{J_0(x)}{R}dx + \frac{1}{R}\frac{1+\mu_{b23}}{1+\mu_{b12}+\mu_{b23}+\mu_{b13}}\right] \quad (126)$$

The first and second integrals in Eq (126) are now over finite intervals of integration and the solutions finite for any values of R. If the Bessel function in the second integration is expanded into its series expansion and integrated term by term, the value of the integral goes to λ_c as $R \rightarrow 0$. The surface integration of the last term in Eq (126) needs to be done analytically for the method of moments analysis. This asymptotic approach is only needed for small R for the Green's functions where the source and observer are on the same plane. The asymptotic approximations are given along with the general form of the Green's functions in Appendix B.

Depending upon the Green's function, the contribution from the last term, which is integrated

analytically, will be entirely real or imaginary. Therefore at least one component of the Green's functions where the source and observer are on the same plane can be approximated for all values of R of interest.

4.1.2 Evaluation Intervals and Antenna Parameters. All the unique Green's functions listed in Table 3 were numerically evaluated using the techniques developed by Nazar. These functions were the ones necessary to describe the tangential electric fields on both antenna patches. All the Green's functions where the source and observer are on the same plane were solved for 50 values of R between 0.001 and 0.1 meters. The asymptotic forms of these functions were solved for 25 values of R between 0 and 0.003 meters. The functions where the source and observer were on different planes were solved for 50 values of R between 0 and 0.1 meters. A quadratic distribution [17, 3] of points was used so that a higher concentration of data points would be taken near R_{min} where the function changes more rapidly. This quadratic distribution can be described by

$$R_i = \frac{(R_{max} - R_{min})}{(N^2 - 1)} (i^2 - 1) + R_{min} \tag{127}$$

where N is the total number of points to evaluate. The functions were evaluated for the following antenna parameters, which were the same as used by Terry in his work [5].

Frequency = 3.7Ghz
$b_{1b} = 0.00158m$
$b_{2b} = 0.00316m$
$\varepsilon_{1b} = 2.2\varepsilon_0$
$\varepsilon_{2b} = 2.2\varepsilon_0$
$\varepsilon_{3b} = \varepsilon_0$
$\mu_{1b} = \mu_{2b} = \mu_{3b} = \mu_0$

The data from the numerical evaluation of the Green's functions was then approximated using the functions described in the next section.

4.2 Green's Function Approximations

The Green's functions are complex valued integral functions. The purpose of this thesis was to determine approximations for the real and imaginary components which could be used in a method of moments analysis. Most functions can not be evaluated exactly even though we may handle them as if they were known exactly. All functions can be approximated by a polynomial or a rational function, which is a polynomial divided by another polynomial [20]. At the outset of this effort it was hoped that polynomial approximations could be used for all the components of the Green's functions, but this was not the case.

All of the Green's functions analyzed had the same general form. They are complex valued functions involving the integration of a Hankel function over an infinite interval. Nazar used a Hankel transform to transform all the Green's functions to integrals of a Bessel function over a semi-infinite interval. The only real difference in the functions is caused by the multiplicative factor in front of the integrand. Some were real and some were imaginary. The Green's functions accounting for the contribution to the **E** field from electric and magnetic surface currents had a real factor out front, while those accounting for the contribution to the **E** field from electric surface charge had an imaginary factor. This can be seen from derivation of the electric scalar potential from magnetic vector potential by using the Lorentz gauge condition (see Eq (77)). As an example $G^{bxx}_{A22}(R)$ and $G^{b}_{q22}(R)$ are shown

$$G^{bxx}_{A22}(R) = \frac{\mu_{1b}}{4\pi}\int_c H_0^{(2)}(\lambda R)\lambda \frac{u_{2b}\cosh(u_{2b}(b_{2b}-b_{1b})) + \mu_{b23}u_{3b}\sinh(u_{2b}(b_{2b}-b_{1b}))}{D^b_e(\lambda)}d\lambda \quad (128)$$

$$G^b_{q22}(R) = \frac{1}{4\pi j\omega\varepsilon_{2b}} \int_c \frac{H_0^{(2)}(\lambda R)\lambda}{D^b_e(\lambda) D^b_m(\lambda)} \left\{ \begin{array}{l} \varepsilon_{b23} u_{2b}^2 u_{3b} \cosh^2(u_{2b}(b_{2b} - b_{1b})) \\ + \left[\begin{array}{c} \mu_{b23} u_{2b}^2 u_{3b} + (\mu_{b12} u_{2b}^2 + \mu_{b13} \varepsilon_{b23} u_{3b}^2) \\ * u_{1b} \tanh(b_{1b} u_{1b}) \end{array} \right] \\ * \sinh^2(u_{2b}(b_{2b} - b_{1b})) \\ + \left[\begin{array}{c} u_{2b}^2 + \mu_{b23} \varepsilon_{b23} u_{3b}^2 + (\mu_{b13} + \mu_{b12} \varepsilon_{b23}) \\ * u_{1b} u_{3b} \tanh(b_{1b} u_{1b}) \end{array} \right] \\ * \frac{u_{2b}}{2} \sinh(2u_{2b}(b_{2b} - b_{1b})) \\ + \mu_{b13} \varepsilon_{b23} u_{1b} u_{2b}^2 \tanh(b_{1b} u_{1b}) \end{array} \right\} d\lambda \quad (129)$$

Notice $G^b_{q22}(R)$ has a 1/j dependence that $G^{bxx}_{A22}(R)$ does not. The net effect of the 1/j factor is to interchange the real and imaginary components and change the sign of the real component. With these differences addressed we can now move to the approximations.

4.2.1 Single Polynomial Approximation. At the outset of this thesis it was hoped to find a polynomial approximation for each component of the Green's functions that would be valid over the entire range of radial separations of interest. This was only possible with half of the components. The graph of the imaginary part of $G^{bxx}_{A22}(R)$ shown in Figure 10 illustrates the behavior where a single polynomial approximation is valid over the entire range of radial separations. The behavior is that of a slowly decaying oscillatory function which can be approximated by a single, sixth order polynomial of the form

$$f(R) = a_0 + a_1 R + a_2 R^2 + a_3 R^3 + a_4 R^4 + a_5 R^5 + a_6 R^6 \quad (130)$$

The sixth order was used to ensure a good fit for all the components of the Green's functions examined.

The approximations were chosen basically by a trial and error method. Several trial form polynomials were chosen and a least squares curve fitting method was used to determine the co-

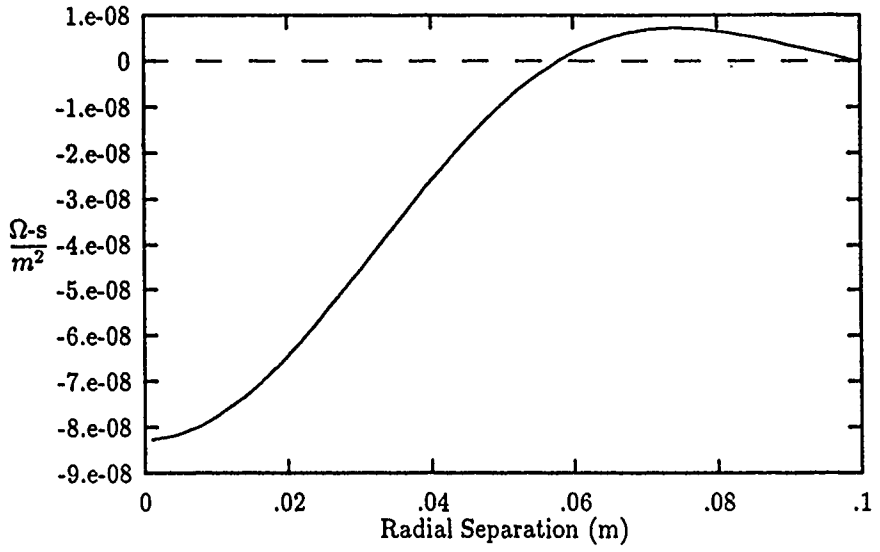

Figure 10. Plot of $G^{bxx}_{A22}(R)$, Imaginary Part.

efficients. The trial polynomials were then evaluated at the same values of radial separation as the original data. Then the original and approximated data were plotted on the same graph and analyzed to see how well they agreed. Several iterations were enough to determine the order of the approximations necessary to match the behavior exhibited in Figure 10.

4.2.2 Piecewise Approximation. The behavior of the other half of the components to be approximated is illustrated by the graph of the real portion of $G^{bxx}_{A22}(R)$ shown in Figure 11. This behavior is that of a sharply decaying oscillatory function. At full scale the oscillatory nature is not evident (see Figure 11a), but if the scale is expanded as in Figure 11b it can be seen. Numerous attempts were made to approximate curves with this behavior by using a single function. Polynomials up to and including tenth order were tried. Good agreement was attained over the sharply declining portion but the oscillatory portion had too much variation.

The interval of interest was broken into two parts. The first was 0.001-0.010 meters. On this interval the function changed the most rapidly and an eighth order polynomial, as shown in

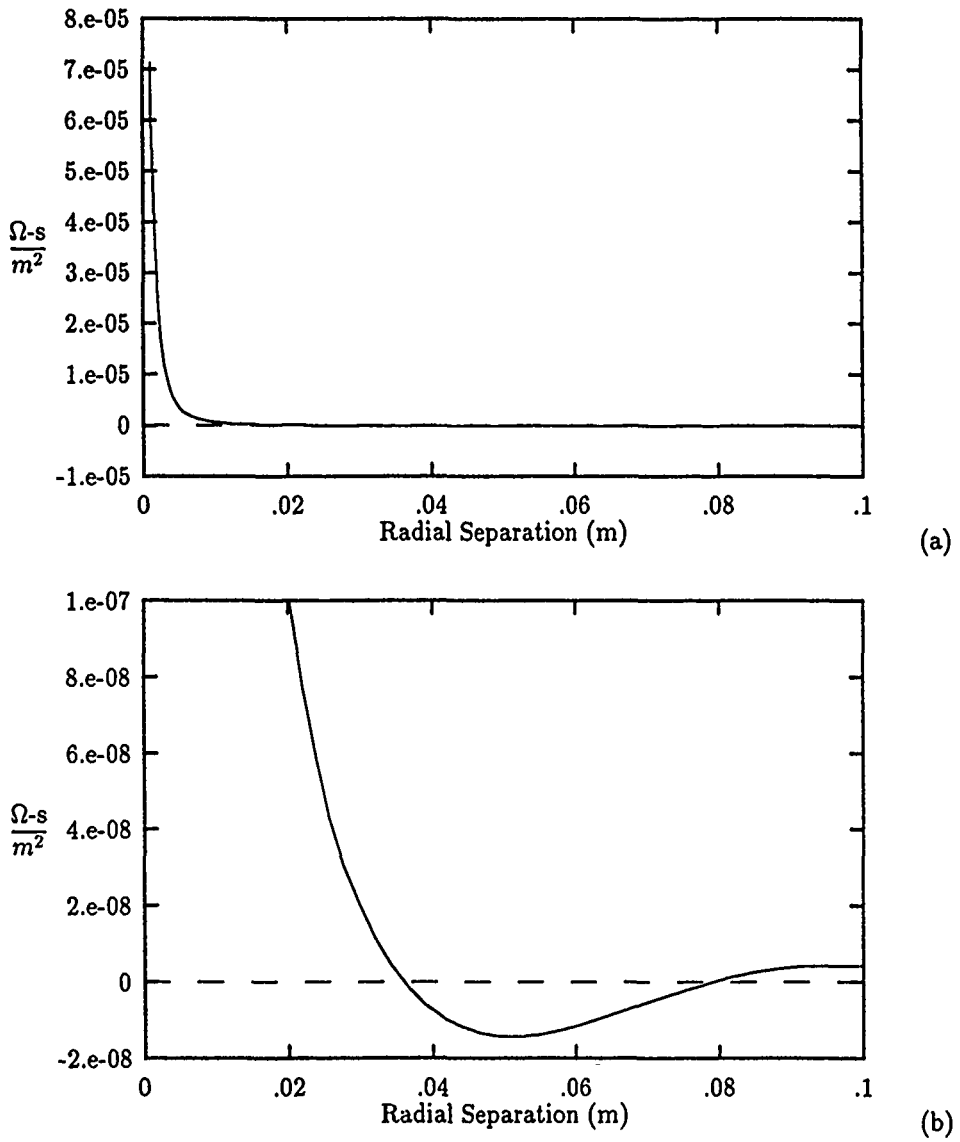

Figure 11. Plot of $G^{bxx}_{A22}(R)$, Real Part,(a) Full Scale, (b) Expanded Scale .

Eq (131), was used to approximate all the Green's functions over this interval. As before the least squares curve fitting method was used to test the different curves and determine the polynomial coefficients. The generality of using a single function for the approximation was lost but it was possible to use the same interval breakpoint for all the Green's functions approximated.

$$g(x) = b_0 + b_1R + b_2R^2 + b_3R^3 + b_4R^4 + b_5R^5 + b_6R^6 + b_7R^7 + b_8R^8 \qquad (131)$$

Over the interval from 0.01 to 0.1 meters the approximating function needed to match the oscillatory nature as well as the remaining portion of the sharply decaying Green's functions. For an arbitrary breakpoint, a simple polynomial would not match the curve. Including several terms with negative powers of R was tried in order to match the sharply decaying portion. These curves were found to be well approximated by an eighth order polynomial plus two terms with negative powers of R. This is actually equivalent to a rational function of two polynomials. The numerator would be a tenth order polynomial and the denominator would be a quadratic polynomial with the constant and first order term equal to zero. Rational functions of polynomials generally give slightly more efficient approximations but are harder to obtain [20]. The coefficients for this approximation were also obtained by using the least squares method with two of the terms having negative powers.

$$h(x) = c_{-1}R^{-1} + c_{-2}R^{-2} + c_0 + c_1R + c_2R^2 + c_3R^3 + c_4R^4 + c_5R^5 + c_6R^6 + c_7R^7 + c_8R^8 \quad (132)$$

A listing of all the Green's functions/components with the form of the applicable approximation for each range is given in Appendix C.

4.3 Sample Results of the Approximations

To show how well the approximations matched the Green's functions, sample plots of the original numerical data with the approximations superimposed are displayed in the next several

sections.

4.3.1 Results for $G^{b22}_{Axx}(R)$ *and* $G^{b}_{q22}(R)$. Plots of $G^{b22}_{Axx}(R)$ and $G^{b}_{q22}(R)$ were chosen to illustrate the behavior of the Green's functions when the source and observer are on the same plane. The Green's functions are plotted from 0.001 - 0.100 meters. The asymptotic expressions were not plotted along with the full expressions. As stated in Section 4.1.1, one component of the asymptotic form is defined at $R = 0$ while the other goes to infinity because of the $1/R$ dependence in the third term of the asymptotic form illustrated in Eq (126).

Figure 12 is a plot of the real portion of $G^{b22}_{Axx}(R)$, both the original and approximated data. Figure 12a is the full scale data and Figure 12b is the expanded data showing the decaying oscillatory nature of the Green's functions. The eighth order and rational polynomials are excellent approximations for the real portion of the function. The imaginary part of $G^{b22}_{Axx}(R)$ is shown in Figure 13. The much more slowly decaying oscillatory nature is well approximated by a sixth order polynomial. The asymptotic form of the imaginary component of $G^{b22}_{Axx}(R)$ is finite at $R = 0$. In fact the value is approximately constant over the range from 0-0.001 meters.

The real portion of $G^{b}_{q22}(R)$ plotted in Figure 14 shows the function is well approximated by a sixth order polynomial. The value of the asymptotic form is almost constant over the range 0-0.001 meters. This behavior can be seen in Figure 14 for values of radial separation close to zero. The plot is of the same shape as the imaginary portion of $G^{b22}_{Axx}(R)$. The switch in the behavior of the real and imaginary components, as compared to $G^{b22}_{Axx}(R)$, is due to the 1/j factor in the Green's function.

The imaginary portion of $G^{b}_{q22}(R)$ is plotted in Figure 15 and is of similar shape to the real part of $G^{b22}_{Axx}(R)$ except for the sign of the values. Here again the eighth order polynomial and the rational polynomial provided excellent approximations for the original function.

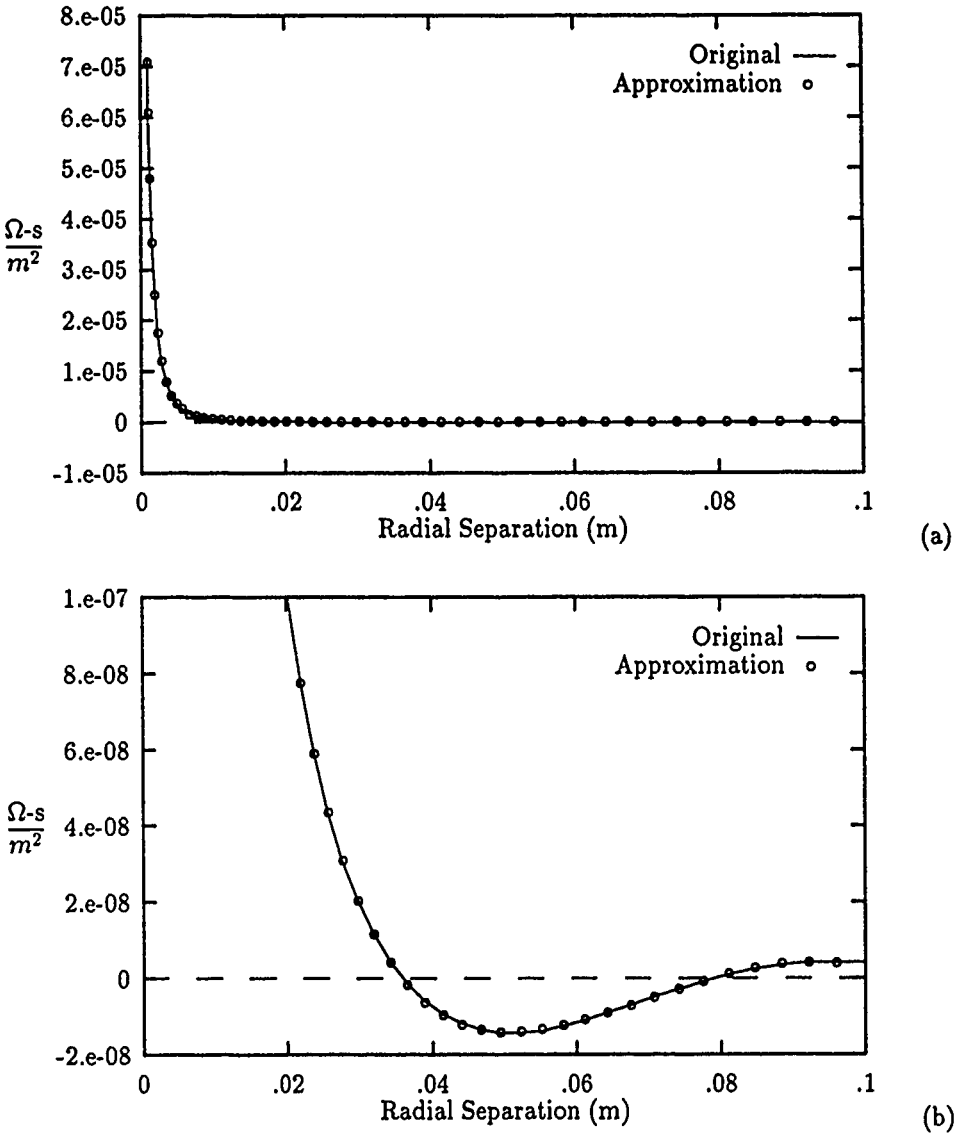

Figure 12. Plot of $G^{bxx}_{A22}(R)$ Real Part,(a) Full Scale, (b) Expanded Scale.

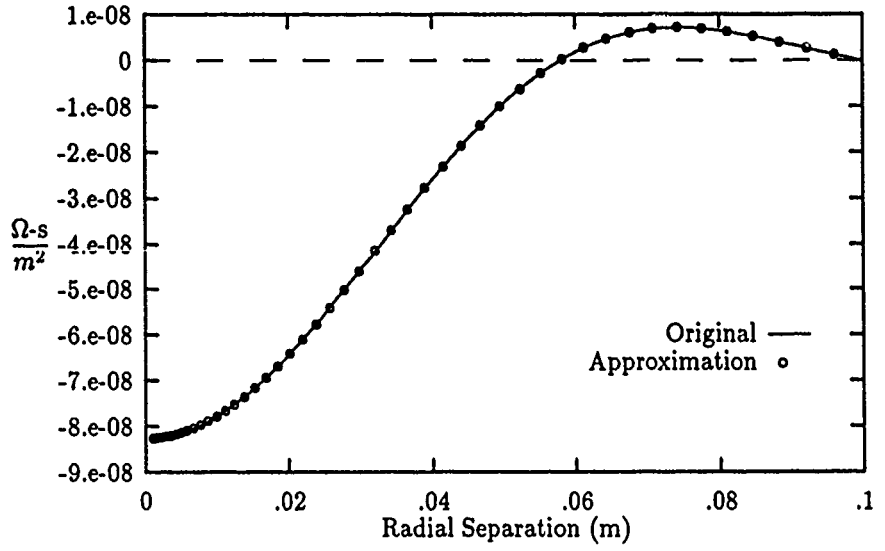

Figure 13. Plot of $G^{bxx}_{A22}(R)$ Imaginary Part .

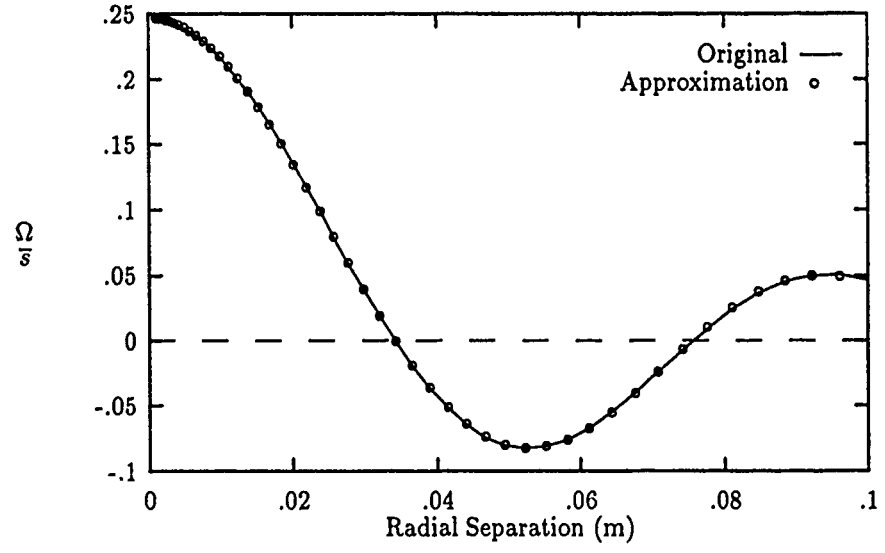

Figure 14. Plot of $G^{b}_{q22}(R)$ Real Part .

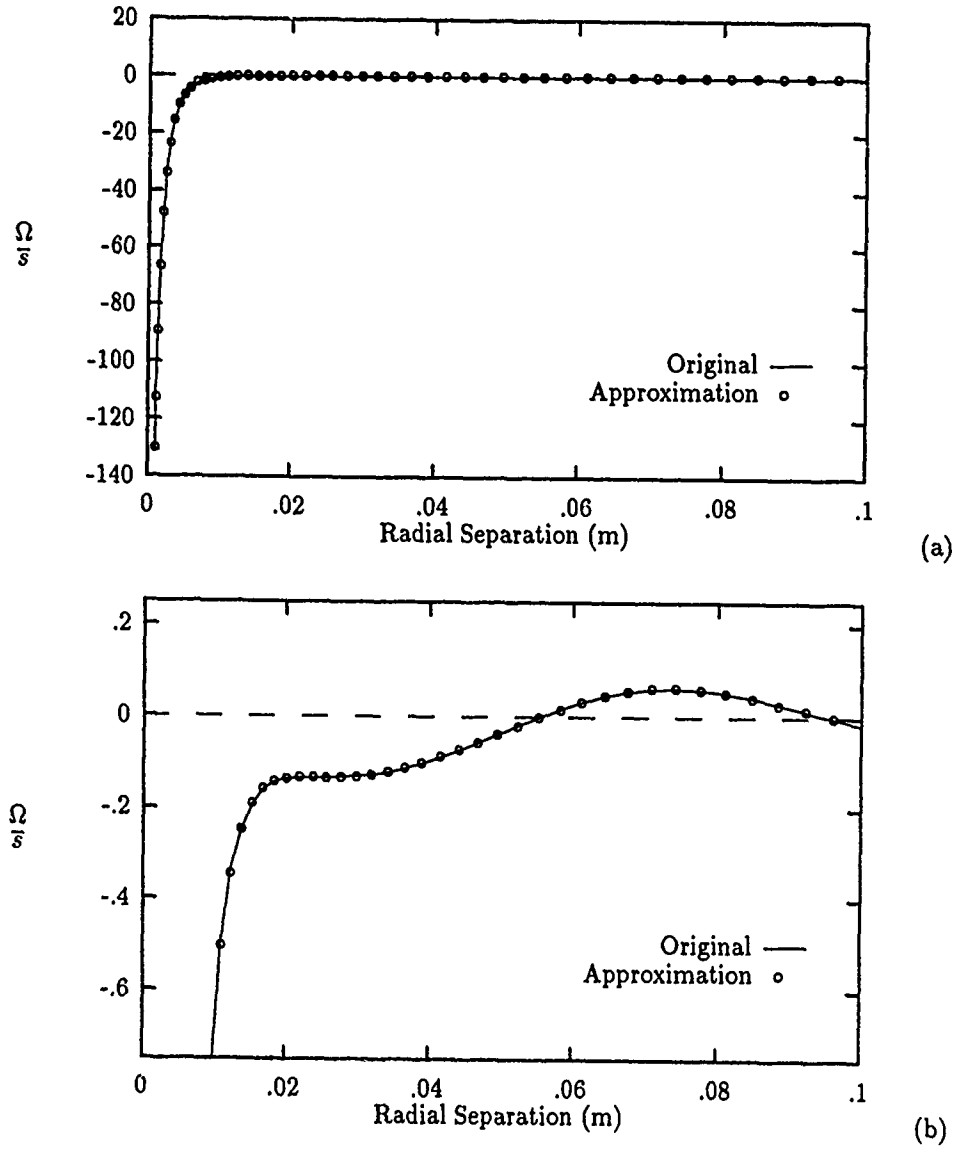

Figure 15. Plot of $G^{b}_{q22}(R)$ Imaginary Part,(a)Full Scale, (b) Expanded Scale.

4.3.2 Results for $G^{b23}_{Axx}(R)$ *and* $G^{b}_{q23}(R)$. Plots of $G^{b23}_{Axx}(R)$ and $G^{b}_{q23}(R)$ were chosen to illustrate the behavior of the Green's functions when the source and observer are on different planes. These functions are plotted from 0 - 0.100 meters and no asymptotic forms were needed.

Figure 16 is a plot of the real portion of $G^{b23}_{Axx}(R)$, both the original and approximated data. Figure 16a is the full scale data and Figure 16b is the expanded data showing the decaying oscillatory nature of the Green's functions. The eighth order and rational polynomials are again excellent approximations for the real portion function.

The imaginary part of $G^{b23}_{Axx}(R)$ shown in Figure 17 is of similar shape as the imaginary part of $G^{b22}_{Axx}(R)$. The much more slowly decaying oscillatory nature is again well approximated by a sixth order polynomial.

The real portion of $G^{b}_{q23}(R)$ is plotted in Figure 18. This function is well approximated by the sixth order polynomial. The plot is of the same shape as the real portion of $G^{b}_{q22}(R)$. Again the switch is due to the 1/j factor in the Green's function.

The imaginary portion of $G^{b}_{q23}(R)$ is plotted in Figure 19 and is of similar shape to the imaginary part of $G^{b}_{q22}(R)$. Here again the eighth order polynomial and the rational polynomial provided excellent approximations for the original.

4.3.3 How Well the Approximations Matched. The initial tests as to how well the approximations matched the Green's functions were done by "eye". The approximations for all the Green's functions basically overlaid the graph of the functions they were to approximate. As a further test of the "goodness" of fit, each function and its approximation was integrated over the entire range of values of R of interest using a simple trapezoidal integration routine. The results of these integrations for the functions displayed in Sections (4.3.1) and (4.3.2) are given in Table 5. The agreement between the actual values and the approximations was excellent. Comparing the actual and approximated results show agreement out to the third or fourth decimal place, indicating agreement to within a fraction of a percentage.

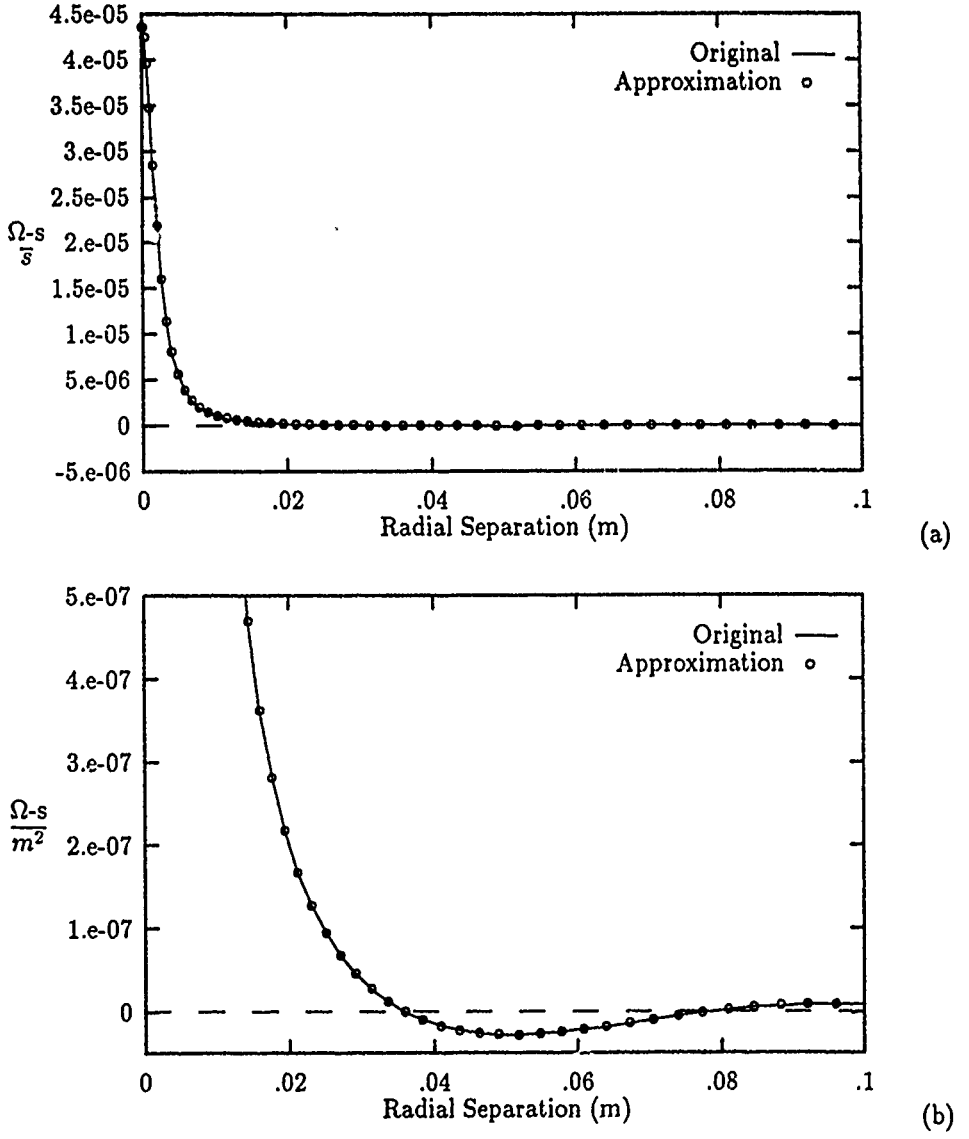

Figure 16. Plot of $G^{bxx}_{A23}(R)$ Real Part, Combined Data (a)Full Scale, (b) Expanded Scale.

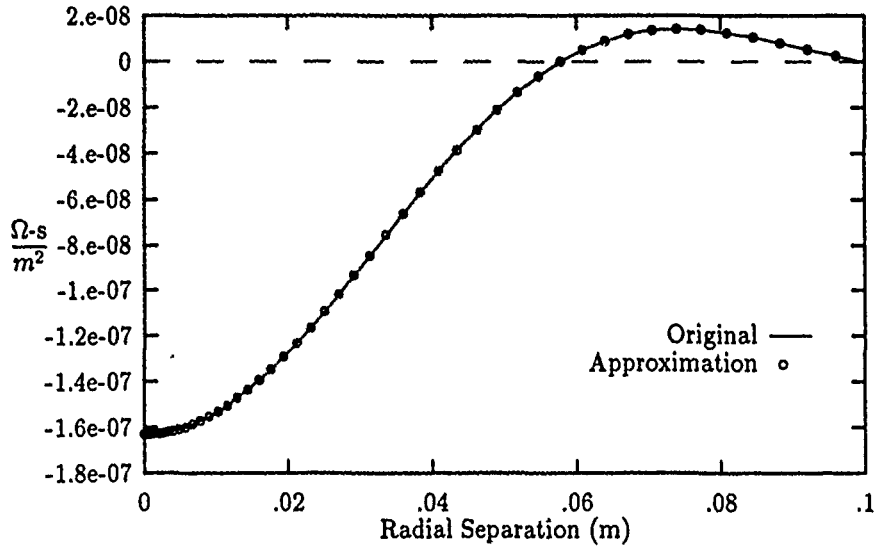

Figure 17. Plot of $G^{bxx}_{A23}(R)$ Imaginary Part, Combined Data .

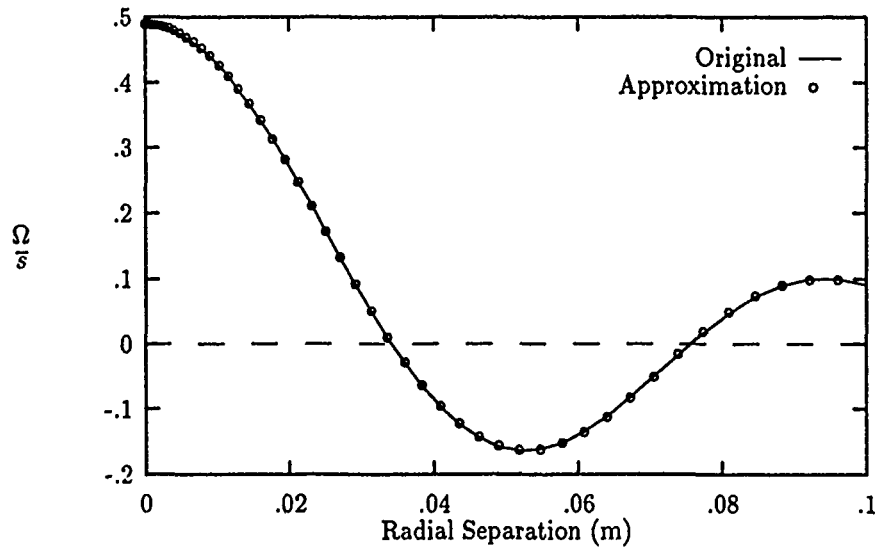

Figure 18. Plot of $G^{b}_{q23}(R)$ Real Part, Combined Data.

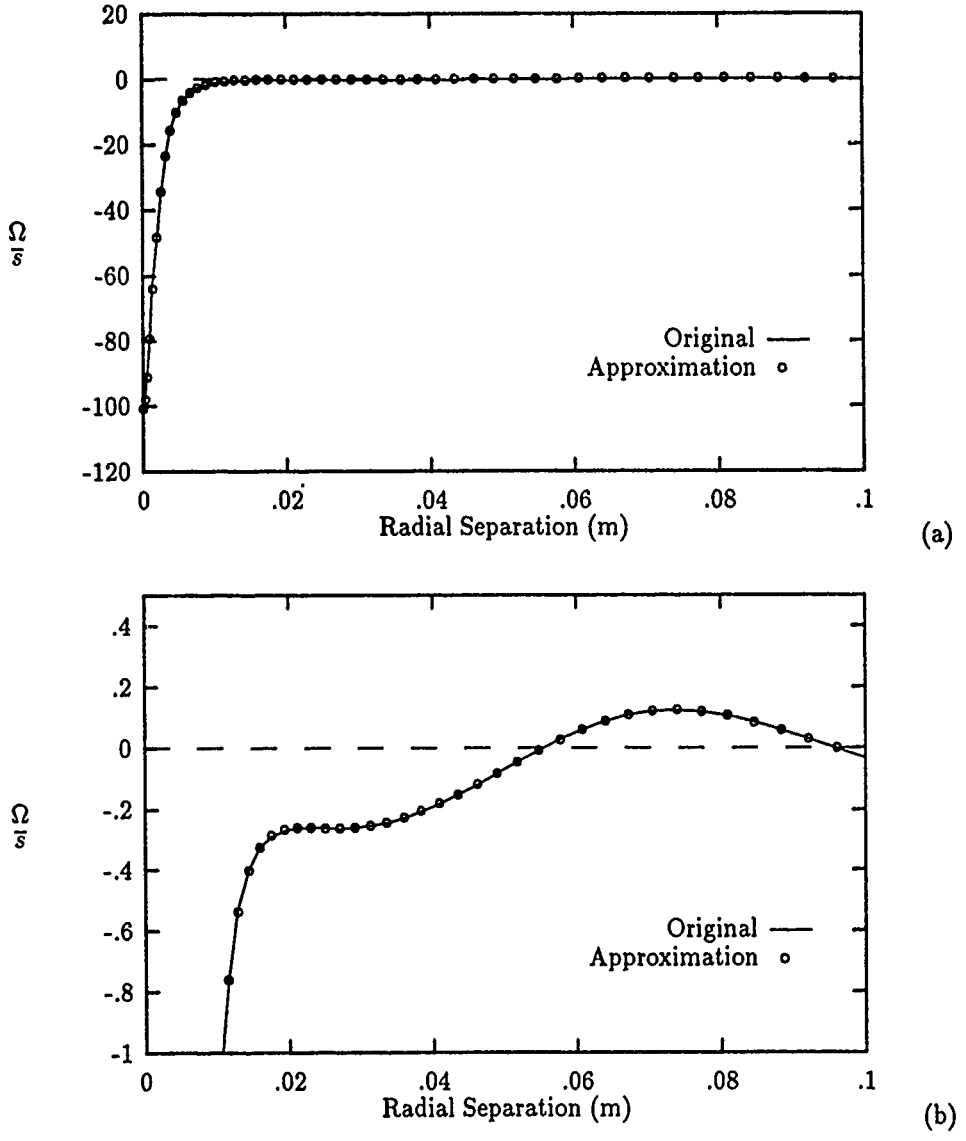

Figure 19. Plot of $G^{b}_{q23}(R)$ Imaginary Part, Combined Data (a)Full Scale, (b) Expanded Scale.

Table 5. Integration of the Green's Functions and their Approximations

Function	Component			
	Real		Imaginary	
	Actual	Approx	Actual	Approx
$G^{bxx}_{A22}(R)$	8.2416e-8	8.2426e-8	-2.3774e-9	-2.3774e-9
$G^{b}_{q22}(R)$	3.5832e-8	3.5817e-8	-1.5358e-1	-1.5359e-1
$G^{bxx}_{A23}(R)$	1.1871e-7	1.1871e-7	-4.8477e-9	-4.8477e-9
$G^{b}_{q23}(R)$	7.5807e-3	7.5776e-3	-2.5025e-1	-2.5025e-1

4.4 Data Supplied to Capt Irvin

The coefficients for the approximations of the full expression Green's functions were given to Capt Irvin for use in his moment method analysis of the antenna. A complete set of the coefficients is given in Appendix C. The data for the asymptotic forms was given to him in tabular form and he interpolated to find any desired value. The handling of the asymptotic data was dictated by time constraints and by some uncertainty at the time about evaluating the asymptotic forms of the Green's functions at $R = 0$. As stated in Section (4.1.1), one component of the approximation could be incorporated into the full expression because it is finite at $R = 0$. The term in the asymptotic approximation with the $1/R$ dependence dominates the behavior of the component which is not finite at $R = 0$. Perhaps the asymptotic data for small values of $R \neq 0$ could be incorporated into the full expression approximation. This would only leave the analytical surface integration of the last term at $R = 0$.

V. Conclusions

Numerical approximations for a theoretical model of an aperture fed stacked-patch microstrip antenna have been developed. The behavior of the Green's functions were examined and three different approximation forms were found applicable to each. The approximations were then used in a separate thesis effort to determine the patch surface currents and charge distributions. The rest of this chapter discusses the answers to the research questions posed in the introduction, suggestions for further work, and some general observations made during the study.

5.1 Answers to Research Questions

5.1.1 What is the form of the functions necessary to accurately model the Green's function? Each Green's function can be modeled by three separate approximations. One component of each Green's function can be modeled with a sixth order polynomial over the entire range of radial separations. The other component required a piece-wise approximation over two separate intervals which were the same for each function. Over the interval from R_{min} out to 0.01 meters, the rapidly changing functions can be modeled by an eighth order polynomial. From 0.01 - 0.10 meters an eighth order polynomial plus two terms with negative powers were used to model the functions. This expression is actually equivalent to a ratio of polynomials with a tenth order polynomial in the numerator and a quadratic polynomial in the denominator.

5.1.2 How well do these functions approximate the original Green's functions? The approximations were found to be excellent approximations for the original Green's functions. When initially developed the "goodness" of fit was determined by "eye" and found that the approximations overlaid the original functions over the entire range of radial separations values of interest. As a further test of the agreement the original functions and the approximations were integrated using a trapezoidal integration routine and the results were found to agree to within at least two

and sometimes and possibly four decimal places. This indicates an error on the order of a fraction of a percent.

5.1.3 Can the approximations be simplified while still retaining the accuracy required for the model? This question was not answered due to lack of time for an iterative process. The actual approximations were determined late in the thesis process and needed by Captain Irvin to complete his thesis effort. Continued work on this question is needed and discussed in the next section.

5.2 Recommended Follow on Work

As mentioned in the previous section, work is needed on determining if simpler approximations would be acceptable in the model. Further work on these approximations needs to be done in concert with the moment method work done by Capt Irvin. Using the approximations developed in this thesis and the surface currents determined by Capt Irvin as a baseline, the effect of simplifying the approximations can be studied. As the radial separation between the source and observer increases, the values of the Green's functions decrease by several orders of magnitude. The effect of determining a lower threshold value of the Green's functions, below which they may be assumed to be zero should be investigated.

Another area of interest would be to take the integration routines written by Nazar and try to simplify them. The IMSL routines used in his code are extremely elaborate. Simpler routines may speed up the numerical evaluations of the Green's functions required for each set of antenna parameters. For example the execution time of the modified Nazar code used in this thesis was one hour on an ELXSI System 6400 Computer, running under its native EMBOS operating system.

The code developed in this thesis needs to be combined into one routine to determine the Green's functions approximations. Separate routines were written for each approximation procedure but the data input was modified to include only the applicable portions. It should be a simple

matter to incorporate the routines into one program with conditionals to determine the appropriate approximations to use.

Appendix A. *Vector Potential Parameters*

A.1 HMD on Interface 1b.

$$N^b_{bx1}(\lambda) = -\varepsilon_{1b}\lambda\left[\varepsilon_{b23}u_{3b}\cosh(b_{2b}u_{2b}) + u_{2b}\sinh(b_{2b}u_{2b})\right]\operatorname{sech}(b_{1b}u_{1b})$$

$$N^b_{cx1}(\lambda) = \varepsilon_{1b}\lambda\left[u_{2b}\cosh(b_{2b}u_{2b}) + \varepsilon_{b23}u_{3b}\sinh(b_{2b}u_{2b})\right]\operatorname{sech}(b_{1b}u_{1b})$$

$$N^b_{dx1}(\lambda) = \varepsilon_{1b}\lambda u_{2b}\exp(b_{2b}u_{3b})\operatorname{sech}(b_{1b}u_{1b})$$

$$N^b_{ex1}(\lambda) = \varepsilon_{1b}\lambda\left\{\begin{array}{l}\left[u_{1b} + \varepsilon_{b13}u_{3b}\tanh(b_{1b}u_{1b})\right]u_{2b}\cosh(u_{2b}(b_{2b} - b_{1b})) \\ + \left[\varepsilon_{b23}u_{1b}u_{3b} + \varepsilon_{b12}u^2_{2b}\tanh(b_{1b}u_{1b})\right]\sinh(u_{2b}(b_{2b} - b_{1b}))\end{array}\right\}$$

$$N^b_{az1}(\lambda) = \varepsilon_{1b}\lambda^2\left\{\begin{array}{l}\left[-\mu_{b13}\varepsilon_{b13} + \cosh^2(u_{2b}(b_{2b} - b_{1b}))\right]2u^2_{2b}\operatorname{csch}(2b_{1b}u_{1b}) \\ + \left[-\mu_{b12}\varepsilon_{b12}u^2_{2b} - \mu_{b13}\varepsilon_{b13}u^2_{3b} + \mu_{b23}\varepsilon_{b23}u^2_{3b}\right] \\ *2\operatorname{csch}(2b_{1b}u_{1b})\sinh^2(u_{2b}(b_{2b} - b_{1b})) \\ + \left[\mu_{b23} - \mu_{b13}\varepsilon_{b12} - \mu_{b12}\varepsilon_{b13} + \varepsilon_{b23}\right] \\ *u_{2b}u_{3b}\operatorname{csch}(2b_{1b}u_{1b})\sinh(2u_{2b}(b_{2b} - b_{1b}))\end{array}\right\}$$

$$N^b_{bz1}(\lambda) = \lambda^2\left\{\begin{array}{l}\left[1 - \mu_{b23}\varepsilon_{b23}\right]\varepsilon_{1b}u_{1b}u_{2b}\operatorname{csch}(b_{1b}u_{1b})\cosh(b_{1b}u_{2b}) \\ \left[-\mu_{b12} + \mu_{b13}\varepsilon_{b23}\right]\varepsilon_{1b}u^2_{2b}\operatorname{sech}(b_{1b}u_{1b})\sinh(b_{1b}u_{2b}) \\ + \left[\begin{array}{l}(\mu_{b13}\varepsilon_{1b} - \mu_{b23}\varepsilon_{2b})u_{3b}\cosh(b_{2b}u_{2b}) \\ +(\mu_{b12}\varepsilon_{1b} - \varepsilon_{2b})u_{2b}\sinh(b_{2b}u_{2b})\end{array}\right] \\ *u_{2b}\operatorname{sech}(b_{1b}u_{1b})\cosh(u_{2b}(b_{2b} - b_{1b})) \\ + \left[\begin{array}{l}(\mu_{b13}\varepsilon_{b13} - \mu_{b23}\varepsilon_{b23})u_{3b}\cosh(b_{2b}u_{2b}) \\ +(\mu_{b12}\varepsilon_{b13} - \varepsilon_{b23})u_{2b}\sinh(b_{2b}u_{2b})\end{array}\right] \\ *\varepsilon_{2b}u_{3b}\operatorname{sech}(b_{1b}u_{1b})\sinh(u_{2b}(b_{2b} - b_{1b}))\end{array}\right\}$$

$$N^b_{cz1}(\lambda) = \lambda^2 \left\{ \begin{array}{l} [1-\mu_{b23}\varepsilon_{b23}]\,\varepsilon_{1b}u_{1b}u_{2b}\mathrm{csch}(b_{1b}u_{1b})\cosh(b_{1b}u_{2b}) \\ [\mu_{b12}+\mu_{b13}\varepsilon_{b23}]\,\varepsilon_{1b}u^2_{2b}\mathrm{sech}(b_{1b}u_{1b})\cosh(b_{1b}u_{2b}) \\ +\left[\begin{array}{l} (-\mu_{b13}\varepsilon_{1b}+\mu_{b23}\varepsilon_{2b})u_{3b}\sinh(b_{2b}u_{2b}) \\ +(-\mu_{b12}\varepsilon_{1b}+\varepsilon_{2b})u_{2b}\cosh(b_{2b}u_{2b}) \end{array} \right] \\ *u_{2b}\mathrm{sech}(b_{1b}u_{1b})\cosh(u_{2b}(b_{2b}-b_{1b})) \\ +\left[\begin{array}{l} (-\mu_{b13}\varepsilon_{b13}+\mu_{b23}\varepsilon_{b23})u_{3b}\sinh(b_{2b}u_{2b}) \\ +(-\mu_{b12}\varepsilon_{b13}+\varepsilon_{b23})u_{2b}\cosh(b_{2b}u_{2b}) \end{array} \right] \\ *\varepsilon_{2b}u_{3b}\mathrm{sech}(b_{1b}u_{1b})\sinh(u_{2b}(b_{2b}-b_{1b})) \end{array} \right\}$$

$$N^b_{dz1}(\lambda) = \exp(b_{2b}u_{3b})u_{2b}\lambda^2 \left\{ \begin{array}{l} [-\mu_{b13}\varepsilon_{1b}+\varepsilon_{3b}]\,u_{2b}\mathrm{sech}(b_{1b}u_{1b})\cosh(u_{2b}(b_{2b}-b_{1b})) \\ +\left[\begin{array}{l} (-\mu_{b23}\varepsilon_{1b}+\varepsilon_{3b}\varepsilon_{b12})u_{1b}\mathrm{csch}(b_{1b}u_{1b}) \\ +(-\mu_{b12}\varepsilon_{1b}+\varepsilon_{2b})u_{3b}\mathrm{sech}(b_{1b}u_{1b}) \end{array} \right] \\ *\sinh(u_{2b}(b_{2b}-b_{1b})) \end{array} \right\}$$

A.2 HED on Interface 2b.

$$N^b_{ax2}(\lambda) = \mu_{1b}\lambda\,[u_{2b}\cosh(u_{2b}(b_{2b}-b_{1b}))+\mu_{b23}u_{3b}\sinh(u_{2b}(b_{2b}-b_{1b}))]\,\mathrm{csch}(b_{1b}u_{1b})$$

$$N^b_{bx2}(\lambda) = -\mu_{1b}\lambda[\mu_{b23}u_{3b}\cosh(b_{2b}u_{2b})+u_{2b}\sinh(b_{2b}u_{2b})]$$

$$N^b_{cx2}(\lambda) = \mu_{1b}\lambda[u_{2b}\cosh(b_{2b}u_{2b})+\mu_{b23}u_{3b}\sinh(b_{2b}u_{2b})]$$

$$N^b_{dx2}(\lambda) = \mu_{1b}\lambda\exp(b_{2b}u_{3b})u_{2b}$$

$$N^b_{az2}(\lambda) = \mu_{1b}\lambda^2 \left\{ \begin{array}{l} [1-\mu_{b13}\varepsilon_{b13}]u^2_{2b}\mathrm{sech}(b_{1b}u_{1b}) \\ +\left[(1-\mu_{b12}\varepsilon_{b12})u^2_{2b}+(-\mu_{b13}\varepsilon_{b13}+\mu_{b23}\varepsilon_{b23})u^2_{3b}\right] \\ *\mathrm{sech}(b_{1b}u_{1b})\sinh^2(u_{2b}(b_{2b}-b_{1b})) \\ +[\mu_{b23}-\mu_{b13}\varepsilon_{b12}-\mu_{b12}\varepsilon_{b13}+\varepsilon_{b23}] \\ *\frac{u_{2b}u_{3b}}{2}\mathrm{sech}(b_{1b}u_{1b})\sinh(2u_{2b}(b_{2b}-b_{1b})) \end{array} \right\}$$

$$N^b_{bz2}(\lambda) = \lambda^2 \left\{ \begin{array}{l} [-\varepsilon_{b12} + \mu_{b23}\varepsilon_{b13}]\mu_{1b}u_{2b}^2 \sinh(b_{1b}u_{2b}) \\ [1 - \mu_{b23}\varepsilon_{b23}]\mu_{1b}u_{1b}u_{2b}\cosh(b_{1b}u_{2b})\tanh(b_{1b}u_{1b}) \\ \left[\begin{array}{l} (\mu_{1b}\varepsilon_{b13} - \mu_{2b}\varepsilon_{b23})u_{3b}\cosh(b_{2b}u_{2b}) \\ +(-\mu_{2b} + \mu_{1b}\varepsilon_{b12})u_{2b}\sinh(b_{2b}u_{2b}) \end{array} \right] \\ *u_{2b}\cosh(u_{2b}(b_{2b} - b_{1b})) \\ + \left[\begin{array}{l} (\mu_{b13}\varepsilon_{b13} - \mu_{b23}\varepsilon_{b23}u_{3b}\cosh(b_{2b}u_{2b}) \\ +(-\mu_{b23} + \mu_{b13}\varepsilon_{b12})u_{2b}\sinh(b_{2b}u_{2b}) \end{array} \right] \\ *\mu_{2b}u_{3b}\sinh(u_{2b}(b_{2b} - b_{1b})) \end{array} \right\}.$$

$$N^b_{cz2}(\lambda) = \lambda^2 \left\{ \begin{array}{l} [\varepsilon_{b12} - \mu_{b23}\varepsilon_{b13}]\mu_{1b}u_{2b}^2 \cosh(b_{1b}u_{2b}) \\ [-1 + \mu_{b23}\varepsilon_{b23}]\mu_{1b}u_{1b}u_{2b}\sinh(b_{1b}u_{2b})\tanh(b_{1b}u_{1b}) \\ \left[\begin{array}{l} (-\mu_{1b}\varepsilon_{b13} + \mu_{2b}\varepsilon_{b23})u_{3b}\sinh(b_{2b}u_{2b}) \\ +(\mu_{2b} - \mu_{1b}\varepsilon_{b12})u_{2b}\cosh(b_{2b}u_{2b}) \end{array} \right] \\ *u_{2b}\cosh(u_{2b}(b_{2b} - b_{1b})) \\ + \left[\begin{array}{l} (-\mu_{b13}\varepsilon_{b13} + \mu_{b23}\varepsilon_{b23})u_{3b}\sinh(b_{2b}u_{2b}) \\ +(\mu_{b23} - \mu_{b13}\varepsilon_{b12})u_{2b}\cosh(b_{2b}u_{2b}) \end{array} \right] \\ *\mu_{2b}u_{3b}\sinh(u_{2b}(b_{2b} - b_{1b})) \end{array} \right\}$$

$$N^b_{dz2}(\lambda) = \exp(b_{2b}u_{3b})u_{2b}\lambda^2 \left\{ \begin{array}{l} [\mu_{3b} - \mu_{1b}\varepsilon_{b13}]u_{2b}\cosh(u_{2b}(b_{2b} - b_{1b})) \\ + \left[\begin{array}{l} (\mu_{2b} - \mu_{1b}\varepsilon_{b12})u_{3b} \\ +(\mu_{3b}\mu_{b12} - \mu_{1b}\varepsilon_{b23})u_{1b}\tanh(b_{1b}u_{1b}) \end{array} \right] \\ *\sinh(u_{2b}(b_{2b} - b_{1b})) \end{array} \right\}$$

A.3 HED on Interface 3b.

$$N^b_{ax3}(\lambda) = \mu_{1b}\lambda u_{2b}\mathrm{csch}(b_{1b}u_{1b})$$

$$N^b_{bx3}(\lambda) = \mu_{2b}\lambda[u_{1b}\cosh(b_{1b}u_{2b})\coth(b_{1b}u_{1b}) - \mu_{b12}u_{2b}\sinh(b_{1b}u_{2b})]$$

$$N^b_{cx3}(\lambda) = \mu_{2b}\lambda[-u_{1b}\sinh(b_{1b}u_{2b})\coth(b_{1b}u_{1b}) + \mu_{b12}u_{2b}\cosh(b_{1b}u_{2b})]$$

$$N^b_{dx3}(\lambda) = \mu_{2b}\lambda\exp(b_{2b}u_{3b})\begin{bmatrix}\mu_{b12}u_{2b}\cosh(u_{2b}(b_{2b}-b_{1b}))\\ +u_{1b}\coth(b_{1b}u_{1b})\sinh(u_{2b}(b_{2b}-b_{1b}))\end{bmatrix}$$

$$N^b_{az3}(\lambda) = \mu_{1b}u_{2b}\lambda^2\left\{\begin{array}{l}[1-\mu_{b13}\epsilon_{b13}]u_{2b}\cosh(u_{2b}(b_{2b}-b_{1b}))\mathrm{sech}(b_{1b}u_{1b})\\ +\begin{bmatrix}(\epsilon_{b12}-\mu_{b23}\epsilon_{b13})u_{1b}\mathrm{csch}(b_{1b}u_{1b})\\ +(-\mu_{b12}\epsilon_{b13}+\epsilon_{b23})u_{3b}\mathrm{sech}(b_{1b}u_{1b})\end{bmatrix}\sinh(u_{2b}(b_{2b}-b_{1b}))\end{array}\right\}$$

$$N^b_{bz3}(\lambda) = \lambda^2\left\{\begin{array}{l}\begin{bmatrix}(\mu_{1b}\epsilon_{b13}-\mu_{2b}\epsilon_{b23})\mu_{3b}\cosh(b_{2b}u_{2b})\\ +(-\mu_{2b}+\mu_{1b}\epsilon_{b12})\mu_{2b}\sinh(b_{2b}u_{2b})\end{bmatrix}u_{2b}\\ +\begin{bmatrix}(-\epsilon_{b12}+\mu_{b23}\epsilon_{b13})u_{2b}\sinh(b_{1b}u_{2b})\\ +(1-\mu_{b23}\epsilon_{b23})u_{1b}\cosh(b_{1b}u_{2b})\tanh(b_{1b}u_{1b})\end{bmatrix}\\ *\mu_{1b}u_{2b}\cosh(u_{2b}(b_{2b}-b_{1b}))\\ +\begin{bmatrix}(1-\mu_{b23}\epsilon_{b23})u_{1b}\cosh(b_{1b}u_{2b})\\ +(-\epsilon_{b12}+\mu_{b23}\epsilon_{b13})u_{2b}\coth(b_{1b}u_{1b})\sinh(b_{1b}u_{2b})\end{bmatrix}\\ *\mu_{2b}u_{1b}\sinh(u_{2b}(b_{2b}-b_{1b}))\end{array}\right\}$$

$$N^b_{cz3}(\lambda) = \lambda^2\left\{\begin{array}{l}\begin{bmatrix}(-\mu_{1b}\epsilon_{b13}+\mu_{2b}\epsilon_{b23})\mu_{3b}\sinh(b_{2b}u_{2b})\\ +(+\mu_{2b}-\mu_{1b}\epsilon_{b12})\mu_{2b}\cosh(b_{2b}u_{2b})\end{bmatrix}u_{2b}\\ +\begin{bmatrix}(\epsilon_{b12}-\mu_{b23}\epsilon_{b13})u_{2b}\cosh(b_{1b}u_{2b})\\ +(-1+\mu_{b23}\epsilon_{b23})u_{1b}\sinh(b_{1b}u_{2b})\tanh(b_{1b}u_{1b})\end{bmatrix}\\ *\mu_{1b}u_{2b}\cosh(u_{2b}(b_{2b}-b_{1b}))\\ +\begin{bmatrix}(-1+\mu_{b23}\epsilon_{b23})u_{1b}\sinh(b_{1b}u_{2b})\\ +(\epsilon_{b12}-\mu_{b23}\epsilon_{b13})u_{2b}\coth(b_{1b}u_{1b})\cosh(b_{1b}u_{2b})\end{bmatrix}\\ *\mu_{2b}u_{1b}\sinh(u_{2b}(b_{2b}-b_{1b}))\end{array}\right\}$$

$$N^{b}_{dz3}(\lambda) = \exp(b_{2b}u_{3b})\lambda^2 \left\{ \begin{array}{l} [-u^2_{1b} + u^2_{2b}]\mu_{3b} \\ + [\mu_{3b}u^2_{1b} - \mu_{1b}\epsilon_{b13}u^2_{2b}] \cosh^2(u_{2b}(b_{2b} - b_{1b})) \\ [-\mu_{2b}\epsilon_{b23}u^2_{1b} + \mu_{3b}\mu_{b12}\epsilon_{b12}u^2_{2b}] \sinh^2(u_{2b}(b_{2b} - b_{1b})) \\ + \left[\begin{array}{l} (\mu_{3b}\epsilon_{b12} - \mu_{2b}\epsilon_{b13})\coth(b_{1b}u_{1b}) \\ +(\mu_{3b}\mu_{b12} - \mu_{1b}\epsilon_{b23})\tanh(b_{1b}u_{1b}) \end{array} \right] \\ * \frac{u_{1b}u_{2b}}{2}\sinh(2u_{2b}(b_{2b} - b_{1b})) \end{array} \right\}$$

Appendix B. *Complete Green's Functions*

$$
\begin{aligned}
D_e^b(\lambda) &= [\mu_{b12}u_{3b} + u_{1b}\coth(b_{1b}u_{1b})]\,u_{2b}\cosh(u_{2b}(b_{2b}-b_{1b})) \\
&\quad + [\mu_{b12}u_{2b}^2 + \mu_{b23}u_{1b}u_{3b}\cot(b_{1b}u_{1b})]\sinh(u_{2b}(b_{2b}-b_{1b})) \\
D_m^b(\lambda) &= [\varepsilon_{b13}u_{3b} + u_{1b}\tanh(b_{1b}u_{1b})]\,u_{2b}\cosh(u_{2b}(b_{2b}-b_{1b})) \\
&\quad + [\varepsilon_{b12}u_{2b}^2 + \varepsilon_{b23}u_{1b}u_{3b}\tan(b_{1b}u_{1b})]\sinh(u_{2b}(b_{2b}-b_{1b}))
\end{aligned}
$$

$$
u_{1b} = \sqrt{\lambda^2 - k_{1b}^2}, \quad u_{2b} = \sqrt{\lambda^2 - k_{2b}^2}, \quad u_{3b} = \sqrt{\lambda^2 - k_{3b}^2}
$$

B.1 Green's Functions for Electric Fields From Electric Sources

B.1.1 HED at Interface 2b.

$$
G_{A22}^{bxx}(R) = \frac{\mu_{1b}}{4\pi}\int_c H_0^{(2)}(\lambda R)\lambda \frac{u_{2b}\cosh(u_{2b}(b_{2b}-b_{1b})) + \mu_{b23}u_{3b}\sinh(u_{2b}(b_{2b}-b_{1b}))}{D_e^b(\lambda)}d\lambda
$$

$$
G_{A22}^{byy}(R) = G_{A22}^{bxx}(R)
$$

$$
G_{q22}^b(R) = \frac{1}{4\pi j\omega\varepsilon_{2b}}\int_c \frac{H_0^{(2)}(\lambda R)\lambda}{D_e^b(\lambda)D_m^b(\lambda)}
\left\{
\begin{array}{l}
\varepsilon_{b23}u_{2b}^2u_{3b}\cosh^2(u_{2b}(b_{2b}-b_{1b})) \\
+\left[\begin{array}{c}\mu_{b23}u_{2b}^2u_{3b} + (\mu_{b12}u_{2b}^2 + \mu_{b13}\varepsilon_{b23}u_{3b}^2) \\ *u_{1b}\tanh(b_{1b}u_{1b})\end{array}\right] \\
*\sinh^2(u_{2b}(b_{2b}-b_{1b})) \\
+\left[\begin{array}{c}u_{2b}^2 + \mu_{b23}\varepsilon_{b23}u_{3b}^2 + (\mu_{b13} + \mu_{b12}\varepsilon_{b23}) \\ *u_{1b}u_{3b}\tanh(b_{1b}u_{1b})\end{array}\right] \\
*\frac{u_{2b}}{2}\sinh(2u_{2b}(b_{2b}-b_{1b})) \\
+\mu_{b13}\varepsilon_{b23}u_{1b}u_{2b}^2\tanh(b_{1b}u_{1b})
\end{array}
\right\}d\lambda
$$

For large λ, these integrands decay as $\lambda^{-1/2}$.

$$G^{bxx}_{A32}(R) = \frac{\mu_{1b}}{4\pi}\int_c H_0^{(2)}(\lambda R)\frac{\lambda u_{2b}}{D^b_e(\lambda)}d\lambda$$

$$G^{byy}_{A32}(R) = G^{bxx}_{A32}(R)$$

$$G^b_{q32}(R) = \frac{1}{4\pi j\omega\varepsilon_{3b}}\int_c \frac{H_0^{(2)}(\lambda R)\lambda u_{2b}}{D^b_e(\lambda)D^b_m(\lambda)}\left\{\begin{array}{l}[u_{3b}+\mu_{b13}u_{1b}\tanh(b_{1b}u_{1b})] \\ *u_{2b}\cosh(u_{2b}(b_{2b}-b_{1b})) \\ +\left[\begin{array}{l}\mu_{b13}\varepsilon_{b12}u^2_{2b}+(\mu_{b23}-\mu_{b13}\varepsilon_{b12})u^2_{3b} \\ +\mu_{b12}u_{1b}u_{3b}\tanh(b_{1b}u_{1b})\end{array}\right] \\ *\sinh(u_{2b}(b_{2b}-b_{1b}))\end{array}\right\}d\lambda$$

For large λ, these integrands decay as $\exp[-\lambda(b_{2b}-b_{1b})]$.

B.1.1.1 Asymptotic Forms for Small R.

$$G^{bxx}_{A22}(R) = \frac{\mu_{1b}}{2\pi}\left\{\int_0^{\lambda_c} I^b_{A22}(R,\lambda)d\lambda - \frac{1+\mu_{b23}}{1+\mu_{b12}+\mu_{b23}+\mu_{b13}}\int_0^{R\lambda_c}\frac{J_0(x)}{R}dx + \frac{1}{R}\frac{1+\mu_{b23}}{1+\mu_{b12}+\mu_{b23}+\mu_{b13}}\right\}$$

$$G^b_{q22}(R) = \frac{1}{2\pi j\omega\varepsilon_{2b}}\left\{\int_0^{\lambda_c} I^b_{q22}(R,\lambda)d\lambda - \frac{1+\varepsilon_{b23}}{1+\varepsilon_{b12}+\varepsilon_{b23}+\varepsilon_{b13}}\int_0^{R\lambda_c}\frac{J_0(x)}{R}dx + \frac{1}{R}\frac{1+\varepsilon_{b23}}{1+\varepsilon_{b12}+\varepsilon_{b23}+\varepsilon_{b13}}\right\}$$

where $I^b_{A22}(R,\lambda)$ and $I^b_{q22}(R,\lambda)$ are the integrands of the original functions with $H_0^{(2)}(\lambda R)$ replaced by $J_0(\lambda R)$.

B.1.2 HED at Interface 3b.

$$G^{bxx}_{A33}(R) = \frac{\mu_{2b}}{4\pi}\int_c \frac{H_0^{(2)}(\lambda R)\lambda}{D^b_e(\lambda)}\left[\begin{array}{l}\mu_{b12}u_{2b}\cosh(u_{2b}(b_{2b}-b_{1b})) \\ +u_{1b}\cot(b_{1b}u_{1b})\sinh(u_{2b}(b_{2b}-b_{1b}))\end{array}\right]d\lambda$$

$$G^{byy}_{A33}(R) = G^{bxx}_{A33}(R)$$

$$G^{b}_{q33}(R) = \frac{1}{4\pi j\omega\varepsilon_{3b}}\int_c \frac{H_0^{(2)}(\lambda R)\lambda}{D^b_e(\lambda)D^b_m(\lambda)}\left\{\begin{array}{l}\left[\begin{array}{l}u_{3b}+\mu_{b13}u_{1b}\tanh(b_{1b}u_{1b})\\ *\cosh^2(u_{2b}(b_{2b}-b_{1b}))\end{array}\right]u^2_{2b}\\ +\left[\begin{array}{l}(u^2_{1b}+\mu_{b12}\varepsilon_{b12}u^2_{2b})\,u_{3b}\\ +\mu_{b23}\varepsilon_{b12}u_{1b}u^2_{2b}\coth(b_{1b}u_{1b})\end{array}\right]\\ *\sinh^2(u_{2b}(b_{2b}-b_{1b}))\\ +\left[\begin{array}{l}\mu_{b23}u^2_{1b}+\mu_{b13}\varepsilon_{b12}u^2_{2b}\\ +\left(\begin{array}{l}\varepsilon_{b12}\coth(b_{1b}u_{1b})\\ +\mu_{b12}\tanh(b_{1b}u1b)\end{array}\right)u_{1b}u_{3b}\end{array}\right]\\ *\frac{u_{2b}}{2}\sinh(2u_{2b}(b_{2b}-b_{1b}))\end{array}\right\}d\lambda$$

For large λ, these integrands decay as $\lambda^{-1/2}$

$$G^{bxx}_{A23}(R) = G^{byy}_{A23}(R) = G^{bxx}_{A32}(R)$$

$$G^{b}_{q23}(R) = \frac{1}{4\pi\omega\varepsilon_{2b}}\int_c \frac{H_0^{(2)}(\lambda R)\lambda u_{2b}}{D^b_e(\lambda)D^b_m(\lambda)}\left\{\begin{array}{l}[(u_{3b}+\mu_{b13}u_{1b}\tanh(b_{1b}u_{1b})]\\ *\varepsilon_{b23}u_{2b}\cosh(u_{2b}(b_{2b}-b_{1b}))\\ +\left[\begin{array}{l}(-1+\mu_{b23}\varepsilon_{b23})u^2_{1b}+u^2_{2b}\\ +\mu_{b12}\varepsilon_{b23}u_{1b}u_{3b}\tanh(b_{1b}u_{1b})\end{array}\right]\\ *\sinh(u_{2b}(b_{2b}-b_{1b}))\end{array}\right\}d\lambda$$

For large λ, these integrands decay as $\exp[-\lambda(b_{2b}-b_{1b})]$.

B.1.2.1 Asymptotic Forms for Small R.

$$G^{bxx}_{A33}(R) = \frac{\mu_{2b}}{2\pi}\left\{\int_0^{\lambda_c} I^b_{A33}(R,\lambda)d\lambda - \frac{1+\mu_{b12}}{1+\mu_{b12}+\mu_{b23}+\mu_{b13}}\int_0^{R\lambda_c}\frac{J_0(x)}{R}dx + \frac{1}{R}\frac{1+\mu_{b12}}{1+\mu_{b12}+\mu_{b23}+\mu_{b13}}\right\}$$

$$G^{b}_{q33}(R) = \frac{1}{2\pi j\omega\varepsilon_{3b}}\left\{\int_0^{\lambda_c} I^{b}_{q33}(R,\lambda)d\lambda - \frac{1+\varepsilon_{b12}}{1+\varepsilon_{b12}+\varepsilon_{b23}+\varepsilon_{b13}}\int_0^{R\lambda_c}\frac{J_0(x)}{R}dx + \frac{1}{R}\frac{1+\varepsilon_{b12}}{1+\varepsilon_{b12}+\varepsilon_{b23}+\varepsilon_{b13}}\right\}$$

where $I^{b}_{A33}(R,\lambda)$ and $I^{b}_{q33}(R,\lambda)$ are the integrands of the original functions with $H_0^{(2)}(\lambda R)$ replaced by $J_0(\lambda R)$.

B.2 Green's Functions for Electric Fields From Magnetic Sources

B.2.1 HMD at Interface 1b.

$$\begin{aligned}
G^{bxx}_{E21}(R,\zeta) &= -\sin(2\zeta)\left[\frac{1}{2}I^{r}_{b21}(R) - I^{s}_{b21}(R)\right]\\
G^{byx}_{E21}(R,\zeta) &= -\left[-I^{t}_{b21}(R) - \cos^2(\zeta)I^{r}_{b21}(R) + \cos(2\zeta)I^{s}_{b21}(R)\right]\\
G^{bxy}_{E21}(R,\zeta) &= -\left[I^{t}_{b21}(R) + \sin^2(\zeta)I^{r}_{b21}(R) + \cos(2\zeta)I^{s}_{b21}(R)\right]\\
G^{byy}_{E21}(R,\zeta) &= -\sin(2\zeta)\left[-\frac{1}{2}I^{r}_{b21}(R) + I^{s}_{b21}(R)\right]
\end{aligned}$$

where

$$I^{r}_{b21}(R) = \int_c \frac{H_0^{(2)}(\lambda R)\lambda^3\operatorname{sech}(b_{1b}u_{1b})}{D^{b}_{e}(\lambda)D^{b}_{m}(\lambda)} * \left\{\begin{array}{l} [1-\mu_{b13}\varepsilon_{b13}]u^2_{2b} \\ +\left[(1-\mu_{b12}\varepsilon_{b12})u^2_{2b} + (-\mu_{b13}\varepsilon_{b13}+\mu_{b23}\varepsilon_{b23})u^2_{3b}\right] \\ *\sinh^2(u_{2b}(b_{2b}-b_{1b})) \\ +[\mu_{b23}-\mu_{b13}\varepsilon_{b12}-\mu_{b12}\varepsilon_{b13}+\varepsilon_{b23}] \\ *\frac{u_{2b}u_{3b}}{2}\sinh(2u_{2b}(b_{2b}-b_{1b})) \end{array}\right\} d\lambda$$

$$I^{s}_{b21}(R) = \int_c \frac{H_1^{(2)}(\lambda R)\lambda^2 \mathrm{sech}(b_{1b}u_{1b})}{RD^b_e(\lambda)D^b_m(\lambda)} * \left\{ \begin{array}{l} [1-\mu_{b13}\epsilon_{b13}]u^2_{2b} \\ +\left[(1-\mu_{b12}\epsilon_{b12})u^2_{2b} + (-\mu_{b13}\epsilon_{b13}+\mu_{b23}\epsilon_{b23})u^2_{3b}\right] \\ *\sinh^2(u_{2b}(b_{2b}-b_{1b})) \\ +[\mu_{b23}-\mu_{b13}\epsilon_{b12}-\mu_{b12}\epsilon_{b13}+\epsilon_{b23}] \\ *\frac{u_{2b}u_{3b}}{2}\sinh(2u_{2b}(b_{2b}-b_{1b})) \end{array} \right\} d\lambda$$

$$I^{t}_{b21}(R) = \int_c \frac{H_0^{(2)}(\lambda R)\lambda u_{2b}\mathrm{sech}(b_{1b}u_{1b})}{D^b_m(\lambda)} \left[\begin{array}{l} \epsilon_{b13}u_{3b}\cosh(u_{2b}(b_{2b}-b_{1b})) \\ +\epsilon_{b12}u_{2b}\sinh(u_{2b}(b_{2b}-b_{1b})) \end{array} \right] d\lambda$$

For large λ, these integrands decay as $\exp(-\lambda b_{1b})$.

$$G^{bxx}_{E31}(R,\zeta) = -\sin(2\zeta)\left[\frac{1}{2}I^{r}_{b31}(R) - I^{s}_{b31}(R)\right]$$

$$G^{byx}_{E31}(R,\zeta) = -\left[-I^{t}_{b31}(R) - \cos^2(\zeta)I^{r}_{b31}(R) + \cos(2\zeta)I^{s}_{b31}(R)\right]$$

$$G^{bxy}_{E31}(R,\zeta) = -\left[I^{t}_{b31}(R) + \sin^2(\zeta)I^{r}_{b31}(R) + \cos(2\zeta)I^{s}_{b31}(R)\right]$$

$$G^{byy}_{E31}(R,\zeta) = -\sin(2\zeta)\left[-\frac{1}{2}I^{r}_{b31}(R) + I^{s}_{b31}(R)\right]$$

where

$$I^{r}_{b31}(R) = \int_c \frac{H_0^{(2)}(\lambda R)\lambda^3}{D^b_e(\lambda)D^b_m(\lambda)} \left\{ \begin{array}{l} [1-\mu_{b13}\epsilon_{b13}]u^2_{2b}\mathrm{sech}(b_{1b}u_{1b})\cosh(u_{2b}(b_{2b}-b_{1b})) \\ +\left[\begin{array}{l} (\epsilon_{b12}-\mu_{b23}\epsilon_{b13})u_{1b}u_{2b}\mathrm{csch}(b_{1b}u_{1b}) \\ +(-\mu_{b12}\epsilon_{b13}+\epsilon_{b23})u_{2b}u_{3b}\mathrm{sech}(b_{1b}u_{1b}) \end{array} \right] \\ *\sinh(u_{2b}(b_{2b}-b_{1b})) \end{array} \right\} d\lambda$$

$$I^{s}_{b31}(R) = \int_c \frac{H^{(2)}_1(\lambda R)\lambda^2}{R D^b_e(\lambda) D^b_m(\lambda)} \left\{ \begin{array}{l} [1-\mu_{b13}\varepsilon_{b13}]u^2_{2b}\mathrm{sech}(b_{1b}u_{1b})\cosh(u_{2b}(b_{2b}-b_{1b})) \\ +\left[\begin{array}{l} (\varepsilon_{b12}-\mu_{b23}\varepsilon_{b13})u_{1b}u_{2b}\mathrm{csch}(b_{1b}u_{1b}) \\ +(-\mu_{b12}\varepsilon_{b13}+\varepsilon_{b23})u_{2b}u_{3b}\mathrm{sech}(b_{1b}u_{1b}) \end{array} \right] \\ *\sinh(u_{2b}(b_{2b}-b_{1b})) \end{array} \right\} d\lambda$$

$$I^{t}_{b31}(R) = \int_c \frac{H^{(2)}_0(\lambda R)\lambda u_{2b}}{D^b_m(\lambda)} [\varepsilon_{b13}u_{3b}\mathrm{sech}(b_{1b}u_{1b})] d\lambda$$

For large λ, these integrands decay as $\exp(-\lambda b_{1b})$.

Appendix C. *Summary of Results*

Green's Function Approximation Forms

$$g(R) = b_0 + b_1R + b_2R^2 + b_3R^3 + b_4R^4 + b_5R^5 + b_6R^6 + b_7R^7 + b_8R^8$$

$$h(R) = c_{-1}R^{-1} + c_{-2}R^{-2} + c_0 + c_1R + c_2R^2 + c_3R^3 + c_4R^4 + c_5R^5 + c_6R^6 + c_7R^7 + c_8R^8$$

$$f(R) = a_0 + a_1R + a_2R^2 + a_3R^3 + a_4R^4 + a_5R^5 + a_6R^6$$

Table 6. Coefficient Order for the Piecewise Approximation

Eighth Order				
b_0	b_1	b_2	b_3	b_4
b_5	b_6	b_7	b_8	
Ratio				
c_{-2}	c_{-1}	c_0	c_1	c_2
c_3	c_4	c_5	c_6	c_7
c_8				

Table 7. Coefficient Order of the Single Function Approximation

Sixth Order				
a_0	a_1	a_2	a_3	a_4
a_5	a_6			

Coefficients for Each Green's Function Approximation

$G^{b22}_{Axx}(R)$

Real Component

8th Order 0.001-0.010
2.8271357E-04 -3.9846556E-01 2.7285907E+02 -1.0962870E+05 2.7278577E+07
-4.2391776E+09 3.9943857E+11 -2.0833405E+13 4.6074276E+14
Ratio 0.010-0.100
1.1336337E-10 -7.7506745E-09 2.8775042E-07 -7.9761966E-14 -2.8113896E-04
1.2917902E-10 3.4524106E-01 -9.6808158E+00 1.2043431E+02 -7.3386638E+02
1.7830531E+03

Imaginary Component

6th Order 0.001-0.100
-8.2697879E-08 3.0039534E-08 4.4481533E-05 3.7821366E-04 -2.3998044E-02
2.3993749E-01 -7.4304513E-01

$G^{b33}_{Axx}(R)$

Real Component

8th Order 0.001-0.010
2.9895392E-04 -3.9713808E-01 2.7003667E+02 -1.0882422E+05 2.7177121E+07
-4.2349631E+09 3.9979300E+11 -2.0878692E+13 4.6215527E+14
Ratio 0.010-0.100
2.6798747E-10 -7.5940224E-09 1.8608318E-07 1.5038343E-14 -3.2242885E-04
-3.1416726E-11 3.4534456E-01 -8.3578282E+00 8.8658536E+01 -4.6285555E+02
9.7745550E+02

Imaginary Component

6th Order 0.001-0.100
-3.2193755E-07 1.1728108E-07 1.7359691E-04 1.4780323E-03 -9.3812439E-02
9.3841354E-01 -2.9073252E+00

$G^{b23}_{Axx}(R)$

Real Component

8th Order 0.000-0.010
4.3605698E-05 1.6428591E-03 -1.9408505E-01 1.0921513E+04 -3.0476872E+06
4.9365870E+08 -4.6983776E+10 2.4369181E+12 -5.3137854E+13
Ratio 0.010-0.100
1.7029449E-10 -8.1399245E-09 2.0622157E-07 -4.1338561E-14 -2.9963275E-04
6.3114878E-11 3.4697986E-01 -9.2439916E+00 1.0942193E+02 -6.3847649E+02
1.4970486E+03

Imaginary Component

6th Order 0.001-0.100
-1.6312406E-07 4.7418351E-08 8.8848203E-05 7.1341936E-04 -4.6862616E-02
4.6971581E-01 -1.4547107E+00

$I^{r}_{b21}(R)$

Real Component

8th Order 0.000-0.010
-2.3690010E+04 -5.1497773E+03 2.0098000E+09 1.1664054E+11 -2.4628222E+14
6.0581647E+16 -6.9634200E+18 4.0033536E+20 -9.2918335E+21
Ratio 0.010-0.100
-2.7567323E-01 4.1969248E+01 -1.7263071E+03 6.7013484E-04 2.5393666E+06
-1.0559782E+00 -3.8054523E+09 1.0860188E+11 -1.3359528E+12 7.9367587E+12
-1.8720567E+13

Imaginary Component

6th Order 0.000-0.100
7.3622798E+02 1.6413327E+02 -9.4660002E+05 -5.5624401E+06 6.6599743E+08
-8.2057805E+09 2.9878758E+10

$I^{s}_{b21}(R)$

Real Component

8th Order 0.000-0.010
-7.1631702E+04 -1.6126649E+06 1.6138582E+10 -4.6090776E+12 2.0514025E+14
1.1322934E+17 -2.2354787E+19 1.6596165E+21 -4.5322535E+22
Ratio 0.010-0.100
-3.9145822E-01 6.0771449E+01 -2.4640424E+03 1.0734826E-03 4.2372332E+06
-1.6926680E+00 -6.5280178E+09 1.8569636E+11 -2.2676061E+12 1.3351982E+13
-3.1213003E+13

Imaginary Component

6th Order 0.000-0.100
1.4578382E+03 3.2605113E+02 -1.8752160E+06 -1.1014941E+07 1.3194275E+09
-1.6258111E+10 5.9202168E+10

$I^{t}_{b21}(R)$

Real Component

8th Order 0.000-0.010
-1.1845706E+04 6.1244112E+03 4.8720618E+08 3.5107918E+10 -4.5628645E+13
9.6364022E+15 -9.8801478E+17 5.1850820E+19 -1.1172704E+21

```
Ratio      0.010-0.100
  -1.4338001E-01  -8.8320753E+00   4.8974870E+02  -1.9777346E-04  -1.6920208E+05
   3.2111913E-01   2.6480174E+08  -9.6649951E+09   1.4729755E+11  -1.0371150E+12
   2.7871008E+12

Imaginary Component

6th Order  0.000-0.100
   3.6839408E+02  -1.0565021E+02  -2.1992704E+05  -1.7804531E+06   1.2335704E+08
  -1.2791397E+09   4.0846293E+09
```

$I^{r}_{b31}(R)$

```
Real Component

8th Order  0.000-0.010
  -3.5845677E+04  -1.8303401E+05   3.3506986E+09  -4.0133292E+11  -1.6475295E+14
   5.8048203E+16  -7.7186016E+18   4.8748677E+20  -1.2131994E+22
Ratio      0.010-0.100
  -3.2220387E-01  -1.1195931E+01   6.7963919E+02  -2.7539833E-04  -7.0817217E+04
   4.4877070E-01   1.6953818E+08  -8.6162929E+09   1.5436197E+11  -1.1848456E+12
   3.3469197E+12

Imaginary Component

6th Order  0.000-0.100
   7.2947448E+02  -2.0927389E+02  -4.3564658E+05  -3.5273908E+06   2.4440619E+08
  -2.5345126E+09   8.0937999E+09
```

$I^{s}_{b31}(R)$

```
Real Component

8th Order  0.000-0.010
   8.3730489E+05   1.8548911E+07  -6.9596640E+11   4.9585244E+14  -1.650909
   3.0643030E+19  -3.2457653E+21   1.8334913E+23  -4.2836938E+24
Ratio      0.010-0.100
   1.0488087E+00  -9.7803738E+01   3.8139458E+03  -1.1916493E-03  -4.5203832E+0
   1.8826109E+00   6.2316114E+09  -1.7672322E+11   2.1844777E+12  -1.3111428E+13
   3.1297587E+13

Imaginary Component

6th Order  0.000-0.100
  -1.2618585E+03  -1.1645510E+01   1.2324177E+06   7.8552878E+06  -8.1658149E+08
   9.7146319E+09  -3.4550352E+10
```

$I^{t}_{b31}(R)$

Real Component

8th Order 0.000-0.010
2.8114574E+05 5.9078765E+06 -5.9241731E+10 1.6899417E+13 -7.7355313E+14
-4.0848676E+17 8.1118069E+19 -6.0339466E+21 1.6495873E+23
Ratio 0.010-0.100
1.5538455E+00 -1.2252199E+02 4.5582187E+03 -1.4436500E-03 -6.4603264E+06
2.2647814E+00 9.1346088E+09 -2.5611943E+11 3.1131480E+12 -1.8348861E+13
4.3053899E+13

Imaginary Component

6th Order 0.000-0.100
-2.4949310E+03 -2.4719206E+01 2.4398514E+06 1.5547730E+07 -1.6171597E+09
1.9242115E+10 -6.8442981E+10

$G^{b}_{q22}(R)$

Real Component

6th Order 0.001-0.100
2.4690865E-01 8.1564715E-02 -3.1310965E+02 -1.7501311E+03 2.1602490E+05
-2.6605711E+06 9.6760956E+06

Imaginary Component

8th Order 0.001-0.010
-5.0295804E+02 6.9944277E+05 -4.7773874E+08 1.9210580E+11 -4.7861591E+13
7.4454262E+15 -7.0205947E+17 3.6635682E+19 -8.1050716E+20
Ratio 0.010-0.100
-3.0506451E-04 3.7573808E-02 -1.5014618E+00 3.1525211E-07 7.9630909E+02
-5.0947594E-04 -7.9604799E+05 2.3725931E+07 -3.2364262E+08 2.1545771E+09
-5.6293092E+09

$G^{b}_{q33}(R)$

Real Component

6th Order 0.001-0.100
9.6785892E-01 3.2169259E-01 -1.2286658E+03 -6.8608196E+03 8.4780207E+05
-1.0443582E+07 3.7986523E+07

Imaginary Component

8th Order 0.001-0.010
-7.1240104E+02 9.5940154E+05 -6.5262043E+08 2.6293123E+11 -6.5657068E+13
1.0231241E+16 -9.6588315E+17 5.0443342E+19 -1.1166002E+21

```
Ratio      0.010-0.100
  -7.3279954E-04   8.4236082E-02  -3.2371602E+00   3.4357684E-07   9.1330452E+02
  -5.4107447E-04  -2.6362783E+05   9.1863973E+06  -1.8340614E+08   1.6197594E+09
  -5.0799782E+09
```

$G^{b}_{q23}(R)$

```
Real Component

6th Order  0.000-0.100
   4.8908078E-01   9.7940015E-02  -6.1506941E+02  -3.6456986E+03   4.3101735E+05
  -5.2961144E+06   1.9249510E+07

Imaginary Component

8th Order  0.000-0.010
  -1.0079854E+02  -3.9690570E+03   4.6810550E+07  -2.6387382E+10   7.3656913E+12
  -1.1930563E+15   1.1354126E+17  -5.8887562E+18   1.2840182E+20
Ratio      0.010-0.100
  -4.6056133E-04   5.4394079E-02  -2.1168582E+00   2.8577567E-07   8.4397927E+02
  -4.4687389E-04  -6.1246793E+05   1.8533381E+07  -2.7071295E+08   1.9286742E+09
  -5.3094692E+09
```

$G^{b}_{q32}(R)$

```
Real Component

6th Order  0.000-0.100
   4.8908078E-01   9.7940015E-02  -6.1506941E+02  -3.6456986E+03   4.3101735E+05
  -5.2961144E+06   1.9249510E+07

Imaginary Component

8th Order  0.000-0.010
  -1.0079854E+02  -3.9690570E+03   4.6810550E+07  -2.6387382E+10   7.3656913E+12
  -1.1930563E+15   1.1354126E+17  -5.8887562E+18   1.2840182E+20
Ratio      0.010-0.100
  -4.6056133E-04   5.4394079E-02  -2.1168582E+00   2.8577567E-07   8.4397927E+02
  -4.4687389E-04  -6.1246793E+05   1.8533381E+07  -2.7071295E+08   1.9286742E+09
  -5.3094692E+09
```

Table 8. Green's Function Approximations Summary

	Real Component		Imaginary Component	
Function	Approximation	Range (m)	Approximation	Range (m)
$G_{Axx}^{b22}(R)$	8th Order Ratio of Polynomials	0.001-0.010 0.010-0.100	6th Order	0.001-0.100
$G_{q22}^{b}(R)$	6th Order	0.001-0.100	8th Order Ratio of Polynomials	0.001-0.010 0.010-0.100
$G_{q32}^{b}(R)$	6th Order	0.000-0.100	8th Order Ratio of Polynomials	0.000-0.010 0.010-0.100
$G_{Axx}^{b33}(R)$	8th Order Ratio of Polynomials	0.001-0.010 0.010-0.100	6th Order	0.001-0.100
$G_{Axx}^{b23}(R)$	8th Order Ratio of Polynomials	0.000-0.010 0.010-0.100	6th Order	0.000-0.100
$G_{q33}^{b}(R)$	6th Order	0.001-0.100	8th Order Ratio of Polynomials	0.001-0.010 0.010-0.100
$G_{q23}^{b}(R)$	6th Order	0.000-0.100	8th Order Ratio of Polynomials	0.000-0.010 0.010-0.100
$I_{b21}^{r}(R)$	8th Order Ratio of Polynomials	0.000-0.010 0.010-0.100	6th Order	0.000-0.100
$I_{b21}^{s}(R)$	8th Order Ratio of Polynomials	0.000-0.010 0.010-0.100	6th Order	0.000-0.100
$I_{b21}^{t}(R)$	8th Order Ratio of Polynomials	0.000-0.010 0.010-0.100	6th Order	0.000-0.100
$I_{b31}^{r}(R)$	8th Order Ratio of Polynomials	0.000-0.010 0.010-0.100	6th Order	0.000-0.100
$I_{b31}^{s}(R)$	8th Order Ratio of Polynomials	0.000-0.010 0.010-0.100	6th Order	0.000-0.100
$I_{b31}^{t}(R)$	8th Order Ratio of Polynomials	0.000-0.010 0.010-0.100	6th Order	0.000-0.100

Appendix D. *Computer Programs*

A description of the programs and subroutines written, modified, and used during this research is presented in this appendix. The programs written by Nazar and modified by the author were run an ELXSI System 6400 computer operating under the ENBOS 13 operating system. The programs written by the author were run on a 20 Mhz PC/AT Clone, Using a Microsoft Version 4.0 FORTRAN compiler. Copies of the actual code may be obtained by contacting

Major Harry Barksdale
AFIT/ENG
Wright-Patterson AFB, OH
45433

D.1 Programs to Numerically Evaluate the Green's Functions

GREENM is the main program used to numerically solve the integrals of all the Green's functions listed in Appendix C. All the material parameters of the antenna are set in GREENM. The original code was written by Nazar [3] and only evaluated representative examples of Green's functions. The author added the code necessary to evaluate remaining Green's functions examined in this thesis. SUBROUT contains all the custom written subroutines called by GREENM. It was also written by Nazar [3] and used with only minor modification. EXTFUN is a file containing all the FORTRAN implementation of the integrands for the various Green's functions and all non-IMSL functions used in GREENM. It also was originally written by Nazar and modified by the author.

D.2 Programs Used to Approximate the Green's Functions

LTSQR6 and LTSQR8 are custom written code which perform a least squares curve fitting using a sixth or and eighth order polynomial. LTSQR82 performs a least squares curve fit using

an eighth order polynomial plus two terms with negative powers. The result is a curve fit using a rational function composed of a tenth order polynomial divided by a quadratic polynomial. All three programs call two subroutines contained in SIMEQ which solve a system of simultaneous linear equations. The routines were extracted from the book *Numerical Recipes* [21]. LTSQR6, LTSQR8, and LTSQR82 were written to only operate on the data from one component of a Green's function at a time. Lack of time prevented consolidation of all the routines. Several file manipulation routines were needed to break out the input file components and combine the results of the approximations.

Bibliography

1. I.J. Bahl and P. Bhartia. *Microstrip Antennas.* Artech House, Inc., Dedham, Massaachusetts, 1980.
2. J.R. James and P.S. Hall. "Introduction." In J.R. James and P.S. Hall, editors, *Handbook of Microstrip Antennas.* Peter Peregrinus LTD, London, 1989.
3. Capt James B. Nazar. *Green's Functions for a Theoretical Model of an Aperture Fed Stacked-Patch Microstrip Antenna.* Master's thesis, School of Engineering, Air Force Institute of Technology (AU), Wright-Patterson AFB OH, December 1989.
4. Capt William L. Irvin. *A Method of Moments Solution for the Electric Currents on an Aperture-Fed Stacked Patch Microstrip Antenna.* Master's thesis, School of Engineering, Air Force Institute of Technology (AU), Wright-Patterson AFB OH, December 1990.
5. Capt Christopher I. Terry. *Establishment of a Fabrication and Measurement Capability for Aperture-Fed Stacked Patch Microstrip Antennas at AFIT.* Master's thesis, School of Engineering, Air Force Institute of Technology (AU), Wright-Patterson AFB OH, December 1990.
6. D.M. Pozar. "Microstrip antenna aperture-coupled to a microstripline." *Electronic Letters,* 21:49–50, January 1985.
7. Peter L. Sullivan and Daniel H. Schaubert. "Analysis of an aperture-coupled microstrip antenna." *IEEE Transactions on Antennas and Propagation,* 34:977–984, August 1986.
8. C.H. Tsao et al. "Aperture-coupled patch antennas with wide-bandwidth and dual polarization capabilities." *1988 IEEE International Symposium Digest Antennas and Propagation,* 3:936–940.
9. Nirod K. Das. *A Study of Multilayered printed Antenna Structures.* PhD thesis, University of Massachusetts, Amherst, MA, 1989.
10. Richard C. Hall and Juan R. Mosig. "The analysis of coaxially fed microstrip antennas with electrically thick substrates." *Electromagnetics,* 9:367–384, 1989.
11. Juan R. Mosig. "Arbitrarily shaped microstrip structures and their analysis with a mixed potential integral equation." *IEEE Transactions on Microwave Theory and Techniques,* 36:314–323, February 1988.
12. J.R. Mosiq and F.E. Gardiol. "Analytical and numerical techniques in the green's function treatment of microstrip antennas and scatterers." *IEE Proceedings, Pt H, No 2,* 130:175–182, March 1983.
13. J.A. Kong. "Antenna radiation in stratified media." In J.A. Kong, editor, *Research Topics in Electromagnetic Wave Theory.* John Wiley & Sons Inc., New York, 1981.
14. Das K. Nirod and David M. Pozar. "A generalized spectral-domain green's function for multilayer dielectric substrates with application to multilayer transmission lines." *IEEE Transactions on Microwave Theory and Techniques,* 35:326–335, March 1987.
15. Roger F. Harrington. *Time-Harmonic Electromagnetic Waves.* McGraw-Hill, New York, 1961.
16. Roger F. Harrington. *Field Computations by Moment Methods.* Robert E. Krieger Publishing Company, Malabar, Florida, 1982.
17. Juan R. Mosig and Fred E. Gardiol. "A dynamical radiation model for microstrip structures." In Peter W. Hawkes, editor, *Advances in Electronics and Electron Physics,* volume 59. Academic Press, New York, 1982.

18. Nicólas G. Alexópoulos and David R. Jackson. "Fundamental superstrate (cover) effects on printed circuit antennas." *IEEE Transactions on Antennas and Propagation*, 32:807–816, August 1984.

19. Peter A. Stark. *Introduction to Numerical Methods.* Macmillan Publishing Co., New York, 1970.

20. Kendal E. Atkinson. *Elementary Numerical Analysis.* John Wiley and Sons, New York, 1885.

21. William H. Press et al. *Numerical Recipes, FORTRAN Version.* Cambridge University Press, New York, 1989.